

**Isotopic compositions of oxygen, iron, chromium, and nickel in cosmic spherules:  
Toward a better comprehension of atmospheric entry heating effects**  
Cécile Engrand<sup>1</sup>, Kevin D. McKeegan<sup>1</sup>, Laurie A. Leshin<sup>1,†</sup>, Gregory F.  
Herzog<sup>2</sup>, Christoph Schnabel<sup>2,‡</sup>, Laurence E. Nyquist<sup>3</sup> and Donald E. Brownlee<sup>4</sup>

<sup>1</sup>Department of Earth and Space Sciences, University of California, Los Angeles, Los Angeles, CA 90095-1567, USA

<sup>2</sup>Department of Chemistry and Chemical Biology, Rutgers University, Piscataway, NJ 08854-8087, USA

<sup>3</sup>NASA Johnson Space Center, Houston, TX 77058, USA

<sup>4</sup>Department of Astronomy, Box 351580, University of Washington, Seattle, WA 98195, USA

Received 14 October 2004; accepted 5 July 2005. Available online 24 December 2005.

**Abstract**

Large, correlated, mass-dependent enrichments in the heavier isotopes of O, Cr, Fe, and Ni are observed in type-I (metal/metal oxide) cosmic spherules collected from the deep sea. Limited intraparticle variability of oxygen isotope abundances, typically <5‰ in  $\delta^{18}\text{O}$ , indicates good mixing of the melts and supports the application of the Rayleigh equation for the calculation of fractional evaporative losses during atmospheric entry. Fractional losses for oxygen evaporation from wüstite, assuming a starting isotopic composition equal to that of air ( $\delta^{18}\text{O} = 23.5\text{‰}$ ;  $\delta^{17}\text{O} = 11.8\text{‰}$ ), are in the range 55%–77%, and are systematically smaller than evaporative losses calculated for Fe (69%–85%), Cr (81%–95%), and especially Ni (45%–99%). However, as  $\delta^{18}\text{O}$  values increase, fractional losses for oxygen approach those of Fe, Cr, and Ni indicating a shift in the evaporating species from metallic to oxidized forms as the spherules are progressively oxidized during entry heating. The observed unequal fractional losses of O and Fe can be reconciled by allowing for a kinetic isotope mass-dependent fractionation of atmospheric oxygen during the oxidation process and/or that some metallic Fe may have undergone Rayleigh evaporation before oxidation began.

In situ measurements of oxygen isotopic abundances were also performed in 14 type-S (silicate) cosmic spherules, 13 from the Antarctic ice and one from the deep sea. Additional bulk Fe and Cr isotopic abundances were determined for two type-S deep-sea spherules. The isotopic fractionation of Cr isotopes suggest appreciable evaporative loss of Cr, perhaps as a sulfide. The oxygen isotopic compositions for the type-S spherules range from  $\delta^{18}\text{O} = -2\text{‰}$  to  $+27\text{‰}$ . The intraspherule isotopic variations are typically small,  $\sim 5\%$  relative, except for the less-heated porphyritic spherules which have preserved large isotopic heterogeneities in at least one case. A plot of  $\delta^{17}\text{O}$  vs.  $\delta^{18}\text{O}$  values for these spherules defines a broad parallelogram bounded at higher values of  $\delta^{17}\text{O}$  by the terrestrial fractionation line, and at lower values of  $\delta^{17}\text{O}$  by a line parallel to it and anchored near the isotopic composition of  $\delta^{18}\text{O} = -2.5\text{‰}$  and  $\delta^{17}\text{O} = -5\text{‰}$ . Lack of independent evidence for substantial evaporative losses suggests that much of this variation reflects the starting isotopic composition of the precursor materials, which likely resembled CO, CM, or CI chondrites. However, the enrichments in heavy isotopes indicate that some mixing with atmospheric oxygen was probably involved during

pdfMachine

Is a pdf writer that produces quality PDF files with ease!

Produce quality PDF files in seconds and preserve the integrity of your original documents. Compatible across nearly all Windows platforms, if you can print from a windows application you can use pdfMachine.

Get yours now!

atmospheric entry for some of the spherules. Isotopic fractionation due to evaporation of incoming grain is not required to explain most of the oxygen isotopic data for type-S spherules. However spherules with barred olivine textures that are thought to have experienced a more intense heating than the porphyritic ones might have undergone some distillation. Two cosmic spherules, one classified as a radial pyroxene type and the other showing a glassy texture, show unfractionated oxygen isotopic abundances. They are probably chondrule fragments that survived atmospheric entry unmelted. Possible reasons type-I spherules show larger degrees of isotopic fractionation than type-S spherules include: a) the short duration of the heating pulse associated with the high volatile content of the type-S spherule precursors compared to type-I spherules; b) higher evaporation temperatures for at least a refractory portion of the silicates compared to that of iron metal or oxide; c) lower duration of heating of type-S spherules compared to type-I spherules as a consequence of their lower densities.

-

## Article Outline

1. [Introduction](#)
2. [Samples and methods](#)
3. [Results of iron-rich \(type I\) Cosmic spherules](#)
  - 3.1. [Sizes, Textures, and Elemental Compositions](#)
  - 3.2. [Oxygen Isotopic Composition](#)
  - 3.3. [Iron Isotopic Composition](#)
  - 3.4. [Chromium and Nickel Isotopic Composition](#)
  - 3.5.  [\$\Phi\$ , a Measure of Overall Mass-Dependent Fractionation](#)
4. [Discussion of type-I spherules](#)
  - 4.1. [Heating Sequence: Hints from Sizes, Textures, and Compositions](#)
  - 4.2. [Evaporative Losses](#)
  - 4.3. [Evaporation Sequence in Type I Spherules](#)
  - 4.4. [Evaporation of Fe and FeO](#)
    - 4.4.1. [Case 1: If the oxygen entering the spherules has  \$\delta^{18}\text{O}\_{\text{SMOW}} = 23.5\text{‰}\$ , i.e., is atmospheric, then evaporation of FeO dominates after 40% of the Fe has evaporated as metallic Fe](#)
    - 4.4.2. [Case 2: If no Fe evaporates as metal, but only as FeO, then the oxygen entering the spherules should have  \$\delta^{18}\text{O}\_{\text{SMOW}\(\text{start}\)} = 12.5\text{‰}\$](#)
    - 4.4.3. [Case 3: If the oxygen entering the spherules has  \$\delta^{18}\text{O}\_{\text{SMOW}\(\text{start}\)} = 15.5\text{‰}\$ , the same value as fusion crusts in iron meteorites, then evaporation of FeO dominates after 12% of the Fe has evaporated as metallic Fe](#)
  - 4.5. [Rarity of Spherules with Little Mass-Dependent Fractionation of Cr and Fe](#)
5. [Results of stony \(type S\) Cosmic spherules](#)
  - 5.1. [Sizes, Textures, and Chemical Compositions](#)
  - 5.2. [Oxygen Isotopic Composition](#)
  - 5.3. [Variability of Oxygen Isotope Composition within Spherules](#)
  - 5.4. [Isotopic Composition of Fe and Cr in Two Type-S Spherules](#)
6. [Discussion of type-S spherules](#)
  - 6.1. [Comparison with Other Oxygen Isotope Data](#)
  - 6.2. [Possible Mechanisms for Setting O Isotope Composition of Spherules](#)

pdfMachine

Is a pdf writer that produces quality PDF files with ease!

Produce quality PDF files in seconds and preserve the integrity of your original documents. Compatible across nearly all Windows platforms, if you can print from a windows application you can use pdfMachine.

Get yours now!

- 6.3. [Relation between Oxygen Isotope Data and Spherule Texture](#)
- 6.4. [Additional Evidence for Small Evaporative Losses of Oxygen from Type S Spherules](#)
- 6.5. [Evaporative Loss from Barred Olivine Spherules](#)
- 6.6. [Isotopically Heterogeneous Spherule 94-4B-43](#)
- 7. [Conclusions](#)
- [Acknowledgements](#)
- [References](#)

## 1. Introduction

Micrometeorites in the size range from 50  $\mu\text{m}$  to 500  $\mu\text{m}$  constitute the dominant source of extraterrestrial material currently accreted by the Earth ([Love and Brownlee, 1993](#)). These particles represent mineralogically, chemically, and isotopically primitive materials (e.g., [Brownlee 1985](#) and [Engrand and Maurette 1998](#)) that have undergone varying degrees of terrestrial alteration, first during atmospheric entry and then during residence in such diverse environments as sea water and Antarctic ice (e.g., [Kurat et al 1994](#) and [Duprat et al 2005](#)).

Rapid atmospheric heating melts many of the incoming particles either partially or completely, thereby producing the cosmic spherules (CS). In this work we examine the effects of this heating on: (1) the isotopic composition of oxygen in both iron-rich (type-I) cosmic spherules and silicate-rich or stony (type-S) cosmic spherules; and (2) the isotopic composition of Cr, Fe, and Ni in type-I CS, and the isotopic composition of Cr in two type-S CS. The changes in isotopic composition are of interest in several contexts. First, because the spherules are flash-heated in the presence of a low pressure gas, isotopic analyses of cosmic spherules may furnish insights into the mechanisms of elemental exchange between chondrule precursors and nebular gas. Second, if the effects of heating are better understood, isotopic analyses may allow the identification of cosmic spherules that formed from chondrules and thereby constrain the abundance of chondrules in the particle flux to Earth. At present that abundance is thought to be very low, <1% (e.g., [Engrand and Maurette, 1998](#)) but is poorly constrained ([Genge 2004](#) and [Genge et al 2005](#)). Third, isotopic analyses may permit estimates of mass loss from cosmic spherules through evaporation and thus aid in refining estimates of the mass distribution of the particle flux to Earth.

Evidence for interesting isotopic behavior of oxygen in *iron-rich* (type-I) cosmic spherules came from the work of [Clayton et al. \(1986\)](#) who reported large positive values of  $\delta^{17}\text{O}$  and  $\delta^{18}\text{O}$  in groups of size-sorted particles. [Davis et al. \(1991\)](#) and [Davis and Brownlee \(1993\)](#) subsequently observed large, mass-dependent enrichments in the heavier isotopes of iron, attributing both them and the previously reported enrichments in oxygen isotopes to evaporation during atmospheric entry. Later studies showed that the isotopes of Ni and Cr were also fractionated and lent support to the idea of evaporative loss (e.g., [Herzog et al., 1999](#), and references therein). Even so, the lack of oxygen isotopic analyses of *individual* type-I cosmic spherules has hampered the estimation of relative elemental evaporation rates and hence has made it more difficult to reconstruct

pdfMachine

Is a pdf writer that produces quality PDF files with ease!

Produce quality PDF files in seconds and preserve the integrity of your original documents. Compatible across nearly all Windows platforms, if you can print from a windows application you can use pdfMachine.

Get yours now!

thermal histories. In this work, we seek to fill the gap by analyzing O, Cr, Fe, and Ni isotopic abundances in several type-I cosmic spherules.

In general, the *stony* or type-S cosmic spherules are thought to preserve the isotopic abundances of the precursor materials more faithfully than do the iron-rich cosmic spherules ([Brownlee et al., 1997](#)). Appreciable mass-dependent isotopic fractionation of Fe, Si, and Mg occurs in a few stony cosmic spherules, however, and to an extent that correlates with independent textural and compositional evidence for heating ([Alexander et al 2002](#) and [Taylor et al 2002](#)). Results for oxygen are fragmentary. [Clayton et al. \(1986\)](#) suggested that the oxygen in melted stony cosmic spherules might be related to the oxygen in bulk C3 chondrites and in the anhydrous components of C2 chondrites. It was not clear from that work how much atmospheric heating might have altered the isotopic abundances of the stony cosmic spherule precursor materials. [Engrand et al. \(1999\)](#) analyzed the oxygen isotopic composition of relict olivine and of relict pyroxene grains in Antarctic micrometeorites (AMMs) that did not melt during atmospheric entry. As did Clayton et al., Engrand and colleagues noted affinity but not identity between the AMMs and carbonaceous chondrites. Their results for these unmelted particles tend to disperse over a wider range than those for any one group of bulk carbonaceous chondrites and to approach the terrestrial fractionation line more closely. Left unsettled by these studies were the respective fractions of the differences owed to variations in the starting composition on the one hand and to the effects of atmospheric heating on the other. By determining the oxygen isotopic compositions of individual stony cosmic spherules and comparing them to the earlier results for unmelted particles, we seek a clearer picture of the effects of heating and melting.

## 2. Samples and methods

Twenty-seven spherules were selected: 11 type-I cosmic spherules (CS) and 3 type-S spherules recovered from deep-sea sediments (DSCS; see [Brownlee, 1985](#)), and 13 type-S spherules collected at Cap Prudhomme in 1994 in Antarctica (ACS; see [Maurette et al., 1994](#)). The DSCS have sizes  $>400\ \mu\text{m}$ ; the ACS are from the  $100\text{--}400\ \mu\text{m}$  size fraction. All samples except two type-S deep-sea spherules (S12 and S13) were mounted in epoxy and polished, and their textures and bulk chemical compositions characterized semi-quantitatively with a scanning electron microscope equipped with an energy-dispersive detector. The major and minor element compositions were determined quantitatively, before any ion microprobe analyses, by using the UCLA CAMECA Camebax microbeam electron microprobe with sample currents set to 10 nA at 15 kV. The detection limit and the analytical uncertainties of the electron microprobe analyses are on the order of 0.01 wt%.

The oxygen isotopic compositions of all samples were measured in situ with the UCLA Cameca ims1270 ion microprobe. Measurements of  $^{16,17,18}\text{O}$  were performed by following the procedure described in [Engrand et al. \(1999\)](#). The diameter of the analysis spot was  $\sim 10\ \mu\text{m}$ . The results are given in the standard  $\delta$  notation relative to Vienna-Standard Mean Ocean Water (V-SMOW, hereafter noted “SMOW”; [Gonfiantini et al., 1993](#), and references therein),  $^{18}\text{O}/^{16}\text{O} = 0.0020052$ , and  $^{17}\text{O}/^{16}\text{O} = 0.00038288$ .

The iron isotopic compositions ( $^{54,56,57}\text{Fe}$ ) were also measured in situ with the UCLA Cameca ims1270 ion microprobe and  $\sim 0.5\ \text{nA}$  primary  $\text{O}^-$  beam, but with a spot size of  $\sim 15\ \mu\text{m}$ . The mass resolving power,  $M/\Delta M \sim 9000$ , was sufficient to resolve  $^{57}\text{Fe}^+$  from the  $^{56}\text{FeH}^+$  interference ([Fahey, 1988](#)). At this mass resolution the correction for the

pdfMachine

Is a pdf writer that produces quality PDF files with ease!

Produce quality PDF files in seconds and preserve the integrity of your original documents. Compatible across nearly all Windows platforms, if you can print from a windows application you can use pdfMachine.

Get yours now!

contribution of the tail of the  $^{56}\text{FeH}^+$  peak to the  $^{57}\text{Fe}^+$  signal is negligible. The  $^{54}\text{Cr}^+$  contribution to the  $^{54}\text{Fe}^+$  signal, typically 1‰-5‰, was removed by measuring the  $^{52}\text{Cr}$  signal and assuming a normal Cr isotopic composition ( $^{53}\text{Cr}/^{52}\text{Cr} = 0.113464$ ,  $^{54}\text{Cr}/^{52}\text{Cr} = 0.028213$ ; [Birck and Allegre, 1985](#)). It is possible to correct for the  $^{54}\text{Cr}$  interference in this way because the samples have low Cr contents, <1%, and because  $^{54}\text{Cr}$  is a minor isotope. We did not try to measure  $^{58}\text{Fe}$  in the face of large interferences from  $^{58}\text{Ni}$ , the major isotope of Ni. The iron isotopic composition is expressed relative to  $^{54}\text{Fe}$  in the standard  $\delta$  notation using the terrestrial iron isotopic ratios of [Völkening and Papanastassiou \(1989\)](#), i.e.,  $^{56}\text{Fe}/^{54}\text{Fe} = 15.956853$  and  $^{57}\text{Fe}/^{54}\text{Fe} = 0.371172$ .

Instrumental fractionation was corrected by assuming a linear mass fractionation law with parameters set for stony CS by analyses of San Carlos olivine, and set for type-I CS by analyses of a natural magnetite standard. We also analyzed the oxygen isotopic composition of a standard containing 10% magnetite and 90% wüstite. No isotopic fractionation (“matrix effect”) was observed between the two types of iron oxides. Several samples were so fine-grained that the analysis of mixed phases was unavoidable—mineral + matrix in the case of the stony CS and magnetite + wüstite for the metallic CS. We made no attempt to correct for possible matrix effects in these cases. The precision of the ion microprobe analyses was 1 to 1.5‰ (1 $\sigma$ ) for both oxygen and iron isotopes, but accuracy could be slightly worse for O isotopes in stony spherules due to mixed-phase matrix effects.

After the ion microprobe measurements of the type-I DSCS were complete, the sample mount was soaked in acetone for a week and the type-I CS removed from the softened material with a stainless steel needle. The polished spherule fragments were weighed, then dissolved in HCl. Cr and Ni in the solution were separated by ion exchange, and an ICP-MS used to measure the Cr, Fe, and Ni contents of the samples. Cr isotopic abundances were determined by thermal ionization mass spectrometry at the Johnson Space Center (see [Nyquist et al., 1994](#)) and Ni isotopic abundances were determined by ICP-MS at Rutgers University (see [Herzog et al., 1999](#)). In addition, Fe isotopic abundances for two type-S spherules (S12 and S13) were determined by TIMS at the Johnson Space Center. The reference ratios for nickel by ICP-MS are:  $^{60}\text{Ni}/^{58}\text{Ni} = 0.385196$ ,  $^{61}\text{Ni}/^{58}\text{Ni} = 0.016746$ ,  $^{62}\text{Ni}/^{58}\text{Ni} = 0.053381$ , and  $^{64}\text{Ni}/^{58}\text{Ni} = 0.013602$ . For chromium and iron, the measured ratios are fractionated from the natural values during evaporation of the sample from the sample filament. This effect is compensated by making the sample and standard “loads” nearly identical, and by following the same filament heating schedule for sample and standard. Reference values for Cr standard are:  $^{50}\text{Cr}/^{52}\text{Cr} = 0.0518585$  (normalizing ratio, [Birck and Allegre, 1985](#));  $^{53}\text{Cr}/^{52}\text{Cr} = 0.113464$  (normalized); and  $^{54}\text{Cr}/^{52}\text{Cr} = 0.028213$  (normalized). Unnormalized values for standards were typically fractionated by 6.4‰/amu and 5.4‰/amu for standard loads of 160 and 80 ng of Cr, respectively. For Fe analyses by TIMS, ratios were measured relative to  $^{56}\text{Fe}$ . The reference values are  $^{54}\text{Fe}/^{56}\text{Fe} = 0.062669$  (normalizing ratio, [Völkening and Papanastassiou, 1989](#));  $^{57}\text{Fe}/^{56}\text{Fe} = 0.0232636$  (normalized); and  $^{58}\text{Fe}/^{56}\text{Fe} = 0.0031103$  (normalized). Unnormalized values for standards were typically fractionated by 9‰/amu for standard loads of 10  $\mu\text{g}$  of Fe. The values for  $\delta^{57}\text{Fe}$  and  $\delta^{56}\text{Fe}$  given in [Table 3](#) are renormalized to  $\delta^{54}\text{Fe} = 0$  from the measured values relative to  $\delta^{56}\text{Fe} = 0$ .

-Table 3.

pdfMachine

Is a pdf writer that produces quality PDF files with ease!

Produce quality PDF files in seconds and preserve the integrity of your original documents. Compatible across nearly all Windows platforms, if you can print from a windows application you can use pdfMachine.

Get yours now!

Iron isotopic composition of nine type-I and two-type-S cosmic spherules from deep-sea sediments. Type-I: by SIMS; Type-S: by TIMS.

Sample	$\delta^{57}\text{Fe} \pm \sigma$ (‰) <sup>‡</sup>	$\delta^{56}\text{Fe} \pm \sigma$ (‰) <sup>‡</sup>
<i>Type-I</i>		
KK2-97A - 1_1	47.0 ± 1.1	33.0 ± 0.7
KK2-97A - 1_1a	46.8 ± 1.1	31.6 ± 0.7
KK2-97A - 1_2a	47.6 ± 1.1	33.6 ± 0.6
KK2-97A - 1_3	48.2 ± 1.6	33.2 ± 1.4
<i>Wtd mean</i>	47.3 ± 0.6	32.8 ± 0.4
KK2-97A - 2_1	30.3 ± 1.1	20.8 ± 1.0
KK2-97A - 2_2	32.5 ± 1.1	23.1 ± 1.0
KK2-97A - 2_3	32.3 ± 1.1	22.8 ± 0.8
<i>Wtd mean</i>	31.7 ± 0.6	22.3 ± 0.5
KK2-97A - 3_1	46.4 ± 1.6	31.9 ± 1.4
KK2-97A - 3_2	45.3 ± 1.6	31.4 ± 1.4
<i>Wtd mean</i>	45.9 ± 1.1	31.6 ± 1.0
KK2-97A - 6_1	41.6 ± 1.1	28.0 ± 0.7
KK2-97A - 6_2	40.3 ± 1.6	26.6 ± 1.5
<i>Wtd mean</i>	41.2 ± 0.9	27.8 ± 0.6
KK2-97A - 7_1	50.7 ± 1.6	34.1 ± 1.4
KK2-97A - 7_2	50.7 ± 1.6	35.0 ± 1.5
<i>Wtd mean</i>	50.7 ± 1.1	34.5 ± 1.0

pdfMachine

Is a pdf writer that produces quality PDF files with ease!

Produce quality PDF files in seconds and preserve the integrity of your original documents. Compatible across nearly all Windows platforms, if you can print from a windows application you can use pdfMachine.

Get yours now!

Sample	$\delta^{57}\text{Fe} \pm \sigma$ (‰) <sup>†</sup>	$\delta^{56}\text{Fe} \pm \sigma$ (‰) <sup>†</sup>
KK2-97A - 8_1	34.7 ± 1.6	21.8 ± 1.5
KK2-97A - 8_2	33.6 ± 1.6	22.2 ± 1.5
KK2-97A - 8_3	31.0 ± 1.6	20.8 ± 1.6
<i>Wtd mean</i>	33.1 ± 0.9	21.6 ± 0.9
KK2-97A - 9_1	49.2 ± 1.1	34.5 ± 0.8
KK2-97A - 9_2	52.0 ± 1.1	36.2 ± 0.7
<i>Wtd mean</i>	50.6 ± 0.8	35.4 ± 0.5
KK2-97A - 10_1	37.7 ± 1.6	25.5 ± 1.4
KK2-97A - 10_2	38.7 ± 1.6	25.6 ± 1.6
<i>Wtd mean</i>	38.2 ± 1.1	25.5 ± 1.1
KK2-97A - 11_1	46.9 ± 1.6	31.5 ± 1.6
KK2-97A - 11_2	49.2 ± 1.6	32.8 ± 1.4
<i>Wtd mean</i>	48.1 ± 1.1	32.2 ± 1.1
<i>Type-S</i>		
S12	4.8 ± 1.0	3.2 ± 0.9
S13	2.0 ± 0.3	1.4 ± 0.3

<sup>†</sup> Delta values are normalized to <sup>54</sup>Fe.

### 3. Results of iron-rich (type I) Cosmic spherules

#### 3.1. Sizes, Textures, and Elemental Compositions

The mean diameters of the type-I particles were measured using transmitted light. They range from  $r_{\text{wd}} = 400 \mu\text{m}$  to  $r_{\text{wd}} = 575 \mu\text{m}$  (Table 1). These diameters are slightly larger than those measured in reflected light, showing that the section was not polished beyond the midsection of the spherules. The textures and chemical compositions of the type-I spherules are comparable to those that [Brownlee \(1985\)](#) described for particles of this

pdfMachine

Is a pdf writer that produces quality PDF files with ease!

Produce quality PDF files in seconds and preserve the integrity of your original documents. Compatible across nearly all Windows platforms, if you can print from a windows application you can use pdfMachine.

Get yours now!

type. In particular, they consist of magnetite (Fe<sub>3</sub>O<sub>4</sub>) intergrown with wüstite (FeO) in different proportions. The presence of wüstite, a metastable phase, indicates high temperature, low oxygen availability, and fast cooling. [Figure 1](#) shows examples of the three typical textures A, B, and C observed in our samples. The abundance of wüstite (light phase on [Fig. 1](#)) decreases from type A to C: in type A, wüstite dominates, magnetite being marginally present; in type B, the proportions of the two phases are approximately the same; in type C, the abundance of magnetite is higher than that of wüstite. Spherules of type B and C are also surrounded by a continuous rim of magnetite, while the type A spherules are not ([Fig. 1](#) and [Table 1](#)).

Table 1.

Diameters (D, μm)<sup>\*</sup>, masses (μg)<sup>§</sup>, textures (Text.)<sup>‡</sup>, magnetite rim thicknesses (Mt, μm)<sup>†</sup>, and chemical compositions (wt %) of type-I cosmic spherules.

Sample	D <sup>*</sup>	Mass <sup>§</sup>	Text. <sup>‡</sup>	Mt <sup>†</sup>	O	Na	Al	Ca	Ti	Cr <sup>‡</sup>	Cr <sup>£</sup>	Mn	Fe <sup>‡</sup>	Fe <sup>£</sup>	Ni <sup>‡</sup>	Ni <sup>£</sup>	Total
KK2-97A -1	505	180	C	25	211	b.d.	0.01	b.d.	0.02	0.06	0.070	0.02	7.28	7.13	0.56	0.50	94.6
KK2-97A -2	440	147	A	0	214	b.d.	0.03	0.03	b.d.	0.03	0.035	0.01	6.89	6.98	5.83	6.70	96.3
KK2-97A -3	408	103	C	20	211	0.01	b.d.	b.d.	b.d.	0.07	0.065	b.d.	7.16	7.55	1.88	1.94	94.7
KK2-97A -4	425	117	C	30	211	0.01	b.d.	0.01	b.d.	0.11	0.100	b.d.	7.31	7.55	0.47	0.43	94.8
KK2-97A -5	443	117	C	20	215	b.d.	0.01	b.d.	b.d.	0.07	0.116	b.d.	7.29	7.19	2.01	1.84	96.5
KK2-97A -6	418	111	B	5	213	b.d.	0.01	0.01	0.01	0.026	0.182	0.01	6.97	7.02	4.46	4.34	95.7
KK2-97A -7	430	116	C	10	211	b.d.	b.d.	0.01	b.d.	0.020	0.145	0.04	6.94	7.05	4.10	4.70	94.9
KK2-97A -8	420	123	A	0	214	b.d.	b.d.	b.d.	0.01	0.08	0.086	0.02	6.92	7.21	5.72	5.96	96.5

Sample	D <sup>*</sup>	Mass <sup>§</sup>	Text. <sup>¥</sup>	Mt <sup>†</sup>	O	Na	Al	Ca	Ti	Cr <sup>‡</sup>	Cr <sup>£</sup>	Mn	Fe <sup>‡</sup>	Fe <sup>£</sup>	Ni <sup>‡</sup>	Ni <sup>£</sup>	Total
-8 (Core)	60		A(N)			b.d.	0.02	0.03	b	0.01		b.d.	7.6		92.7		100.3
KK2-97A -9	555	224	C	30	21.4	b.d.	b.d.	b.d.	b.d.	0.07	0.071	b.d.	74.0	76.6	0.47	0.42	95.9
KK2-97A -10	575	385	B	3	21.5	b.d.	0.01	b.d.	0.01	0.025	0.259	0.04	69.5	69.3	5.5	5.56	96.8
KK2-97A -11	485	157	C	20	21.3	b.d.	0.04	0.05	b.d.	0.07	0.134	0.03	73.4	76.3	0.63	0.66	95.6
Average										0.12	0.11	0.02	71.3	72.6	2.9	3.0	
$\sigma$										0.08	0.06	0.01	2.0	2.8	2.3	2.5	
Literature <sup>&amp;</sup>										0.16			68.4		2.5		

b.d.: below detection limit of  $\sim 0.01$  wt%.

<sup>\*</sup> Average diameters (in  $\mu\text{m}$ ) were measured on polished sections using transmitted light.

<sup>§</sup> The polished spherules were weighed after extraction from epoxy. Diameters measured on the polished section by reflected light only slightly larger than those measured using transmitted light suggest that the spherules were polished almost to their half.

<sup>¥</sup> The letters A, B, and C refer to the textures shown in [Figures 1A](#) (magnetite dendrites in wüstite), [1B](#) (magnetite in higher abundance but not dendritic), and [1C](#) (exsolution of magnetite in wüstite). The letter N signifies the presence of a core (nugget).

<sup>†</sup> Thickness (in  $\mu\text{m}$ ) of a layer of pure magnetite that rims some, but not all spherules.

<sup>‡</sup> Electron microprobe analysis.

<sup>£</sup> ICP-MS analysis.

<sup>&</sup> Weighted average based on [Herzog et al. \(Table 3; 1999\)](#).

-

pdfMachine

Is a pdf writer that produces quality PDF files with ease!

Produce quality PDF files in seconds and preserve the integrity of your original documents. Compatible across nearly all Windows platforms, if you can print from a windows application you can use pdfMachine.

Get yours now!



(330K)

Fig. 1. Backscattered electron micrographs of the three textures observed in the section KK2-97A of type-I deep-sea cosmic spherules. There is a systematic increase in the abundance of magnetite ( $\text{Fe}_3\text{O}_4$ , dark phase) over wüstite ( $\text{FeO}$ , light phase) from type A to type C. (A) Spherule showing magnetite dendrites in wüstite. Wüstite is the most abundant phase. A metal core (92.5 wt% Ni, 7.5 wt% Fe) is visible in the plane of the section; (B) spherule showing about the same proportion of magnetite and wüstite phases. The spherule exhibits a rim of pure magnetite. Magnetite does not have a dendritic texture; (C) exsolution of magnetite in wüstite with a thick rim of magnetite. The abundance of magnetite is well above that of wüstite. These textural differences are probably due to differences in heating and cooling rates: the temperatures and duration of heating probably increased in the order  $A < B < C$ .

The Cr, Fe, and Ni contents, as measured independently by averaging spot analyses with the electron microprobe and by ICP-MS (bulk analysis), agree well (Table 1). The iron contents of the oxides slightly increase from type A to type C spherules, averaging  $\sim 72$  wt% Fe, while their nickel contents decrease from type A to C (Table 1). In relative terms, the nickel contents vary more, from 0.5 wt% in type C to  $\sim 6$  wt% in type A, than do the iron contents. One spherule (spherule 8) has a nickel rich metal core (92.5 wt% Ni, 7.5 wt% Fe) in the plane of the polished section (Fig. 1A). There are no systematic variations of the chromium contents with the textural types. They range from the detection limit of  $\sim 0.01$  wt% in the metal core of spherule 8 to a high of  $\sim 0.26$  wt% in spherule 6 (Table 1).

### 3.2. Oxygen Isotopic Composition

Table 2 shows the oxygen isotopic compositions measured relative to standard mean ocean water (SMOW) for two to ten spots in each of eleven type-I spherules. The data fall along the terrestrial fractionation line (TF),  $\delta^{17}\text{O} \sim 0.52 \times \delta^{18}\text{O}$ , with  $\delta^{18}\text{O}$  values ranging from 38.4‰ to 57.4‰, and  $\delta^{17}\text{O}$  values from 19.1‰ to 29.4‰ (Fig. 2). The mean values for our analyses,  $\delta^{18}\text{O} = 47.0 \pm 5.5\text{‰}$  and  $\delta^{17}\text{O} = 23.9 \pm 2.9\text{‰}$ , are consistent with those of Clayton et al. (1986), which fell in a narrower range,  $39.9\text{‰} < \delta^{18}\text{O} < 47.1\text{‰}$ . For different spots within individual spherules the measured values of  $\delta^{18}\text{O}$  vary by only a small amount, from 0.3‰ (Table 2, spherule 4) to 6.8‰ (Table 2, spherule 7).

Table 2.

Oxygen isotopic composition measured by ion microprobe of eleven type-I cosmic spherules from deep-sea sediments.

Sample	Text.*	$\delta^{18}\text{O} \pm 1\sigma$ (‰) <sup>†</sup>	$\delta^{17}\text{O} \pm 1\sigma$ (‰) <sup>†</sup>	$\Delta^{17}\text{O} \pm 1\sigma$ (‰) <sup>‡‡</sup>
KK2-97A-1_1		$56.7 \pm 1.0$	$29.4 \pm 0.8$	$0.0 \pm 1.1$
KK2-97A-1_2		$54.2 \pm 1.0$	$27.5 \pm 1.1$	$-0.7 \pm 1.3$

pdfMachine

Is a pdf writer that produces quality PDF files with ease!

Produce quality PDF files in seconds and preserve the integrity of your original documents. Compatible across nearly all Windows platforms, if you can print from a windows application you can use pdfMachine.

Get yours now!

Sample	Text.*	$\delta^{18}\text{O} \pm 1\sigma$ (‰) <sup>†</sup>	$\delta^{17}\text{O} \pm 1\sigma$ (‰) <sup>†</sup>	$\Delta^{17}\text{O} \pm 1\sigma$ (‰) <sup>‡‡</sup>
<i>Wtd mean</i>	<i>C</i>	$55.5 \pm 0.7$	$28.8 \pm 0.6$	$-0.3 \pm 0.8$
KK2-97A-2_1		$42.9 \pm 0.9$	$20.4 \pm 1.0$	$-1.9 \pm 1.2$
KK2-97A-2_2		$38.4 \pm 1.0$	$19.5 \pm 1.1$	$-0.5 \pm 1.3$
<i>Wtd mean</i>	<i>A</i>	$40.8 \pm 0.7$	$20.0 \pm 0.7$	$-1.2 \pm 0.9$
KK2-97A-3_1		$48.7 \pm 0.9$	$23.5 \pm 0.9$	$-1.8 \pm 1.1$
KK2-97A-3_2		$45.8 \pm 0.9$	$22.2 \pm 1.0$	$-1.6 \pm 1.2$
KK2-97A-3_3		$46.4 \pm 0.9$	$22.3 \pm 1.1$	$-1.8 \pm 1.3$
KK2-97A-3_4		$46.3 \pm 0.9$	$22.4 \pm 1.0$	$-1.7 \pm 1.2$
KK2-97A-3_5		$46.2 \pm 0.9$	$24.3 \pm 1.1$	$0.3 \pm 1.3$
<i>Wtd mean</i>	<i>C</i>	$46.7 \pm 0.4$	$23.0 \pm 0.4$	$-1.4 \pm 0.5$
KK2-97A-4_1		$50.2 \pm 0.9$	$24.9 \pm 1.0$	$-1.2 \pm 1.2$
KK2-97A-4_2		$49.9 \pm 0.9$	$24.5 \pm 0.9$	$-1.4 \pm 1.1$
<i>Wtd mean</i>	<i>C</i>	$50.0 \pm 0.6$	$24.7 \pm 0.7$	$-1.3 \pm 0.8$
KK2-97A-5_1		$49.1 \pm 0.9$	$24.7 \pm 0.9$	$-0.9 \pm 1.1$
KK2-97A-5_2		$47.7 \pm 0.9$	$24.1 \pm 1.0$	$-0.7 \pm 1.2$
<i>Wtd mean</i>	<i>C</i>	$48.4 \pm 0.6$	$24.4 \pm 0.7$	$-0.8 \pm 0.8$
KK2-97A-6_1		$39.2 \pm 1.1$	$19.2 \pm 0.9$	$-1.3 \pm 1.0$
KK2-97A-6_2		$44.3 \pm 1.0$	$23.1 \pm 0.9$	$0.0 \pm 1.0$
KK2-97A-6_3		$39.0 \pm 1.0$	$20.6 \pm 0.9$	$0.3 \pm 1.0$
<i>Wtd mean</i>	<i>B</i>	$40.9 \pm 0.6$	$20.9 \pm 0.5$	$-0.3 \pm 0.6$

pdfMachine

Is a pdf writer that produces quality PDF files with ease!

Produce quality PDF files in seconds and preserve the integrity of your original documents. Compatible across nearly all Windows platforms, if you can print from a windows application you can use pdfMachine.

Get yours now!

Sample	Text.*	$\delta^{18}\text{O} \pm 1\sigma$ (‰) <sup>†</sup>	$\delta^{17}\text{O} \pm 1\sigma$ (‰) <sup>†</sup>	$\Delta^{17}\text{O} \pm 1\sigma$ (‰) <sup>‡‡</sup>
KK2-97A-7_1		45.9 ± 0.9	24.2 ± 0.9	0.4 ± 1.0
KK2-97A-7_1b		46.6 ± 0.9	24.4 ± 0.8	-0.8 ± 1.0
KK2-97A-7_2		45.6 ± 0.9	22.9 ± 0.9	-1.2 ± 1.2
KK2-97A-7_3		42.2 ± 1.0	20.8 ± 1.1	1.2 ± 1.1
KK2-97A-7_4		42.8 ± 1.0	23.5 ± 1.0	0.4 ± 1.2
KK2-97A-7_5		46.0 ± 0.9	24.3 ± 1.1	-0.8 ± 1.2
KK2-97A-7_6		47.4 ± 0.9	23.9 ± 1.1	0.7 ± 1.2
KK2-97A-7_7		48.2 ± 1.0	25.8 ± 1.1	0.7 ± 1.2
KK2-97A-7_8		48.9 ± 0.9	26.1 ± 1.2	-0.3 ± 1.1
KK2-97A-7_9		47.8 ± 0.9	24.5 ± 1.0	0.1 ± 1.0
<i>Wtd mean</i>	<i>C</i>	<i>46.2 ± 0.3</i>	<i>24.0 ± 0.3</i>	<i>0.0 ± 0.3</i>
KK2-97A-8_1		42.5 ± 1.0	22.6 ± 1.1	0.5 ± 1.2
KK2-97A-8_2		41.9 ± 1.1	21.8 ± 1.1	0.0 ± 1.2
KK2-97A-8_3		41.7 ± 1.0	21.7 ± 0.9	0.0 ± 1.0
<i>Wtd mean</i>	<i>A</i>	<i>42.0 ± 0.6</i>	<i>22.0 ± 0.6</i>	<i>0.2 ± 0.7</i>
KK2-97A-9_1		57.4 ± 0.9	29.3 ± 0.9	-0.6 ± 1.0
KK2-97A-9_2		52.1 ± 1.0	25.8 ± 1.0	-1.3 ± 1.1
KK2-97A-9_3		55.5 ± 1.0	26.8 ± 1.1	-2.0 ± 1.2
KK2-97A-9_4		56.8 ± 0.9	29.0 ± 0.9	-0.5 ± 1.0
<i>Wtd mean</i>	<i>C</i>	<i>55.6 ± 0.5</i>	<i>27.9 ± 0.5</i>	<i>-1.0 ± 0.5</i>
KK2-97A-10_1		41.5 ± 0.9	21.7 ± 1.0	0.2 ± 1.1

pdfMachine

Is a pdf writer that produces quality PDF files with ease!

Produce quality PDF files in seconds and preserve the integrity of your original documents. Compatible across nearly all Windows platforms, if you can print from a windows application you can use pdfMachine.

Get yours now!

Sample	Text.* <sup>‡</sup>	$\delta^{18}\text{O} \pm 1\sigma$ (‰) <sup>†</sup>	$\delta^{17}\text{O} \pm 1\sigma$ (‰) <sup>†</sup>	$\Delta^{17}\text{O} \pm 1\sigma$ (‰) <sup>‡‡</sup>
KK2-97A-10_2		$39.8 \pm 1.0$	$19.8 \pm 0.9$	$-0.9 \pm 1.1$
KK2-97A-10_3		$43.9 \pm 1.0$	$22.6 \pm 1.0$	$-0.3 \pm 1.1$
KK2-97A-10_4		$40.2 \pm 0.9$	$21.1 \pm 0.9$	$0.2 \pm 1.0$
<i>Wtd mean</i>	A	$41.3 \pm 0.5$	$21.2 \pm 0.5$	$-0.2 \pm 0.5$
KK2-97A-11_1		$49.0 \pm 0.9$	$26.8 \pm 0.9$	$1.3 \pm 1.0$
KK2-97A-11_2		$50.0 \pm 0.9$	$26.2 \pm 1.0$	$0.2 \pm 1.1$
KK2-97A-11_3		$50.4 \pm 0.9$	$26.2 \pm 0.9$	$-0.1 \pm 1.0$
<i>Wtd mean</i>	A	$49.8 \pm 0.5$	$26.4 \pm 0.5$	$0.5 \pm 0.6$

<sup>‡</sup> See [Figure 1](#) and caption [Table 1](#)

<sup>†</sup> Relative to SMOW, errors are  $1\sigma$  mean.

<sup>‡‡</sup>  $\Delta^{17}\text{O} = \delta^{17}\text{O} - 0.52 \times \delta^{18}\text{O}$

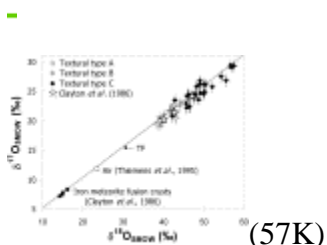


Fig. 2. Oxygen isotope abundances in type-I spherules plot along a mass-dependent fractionation line. The terrestrial fractionation line (TF) passes through both the composition of air (open circle; data taken from [Thiemens et al., 1995](#)), and of standard mean ocean water (SMOW). Our data are shown according to the three textural types (A, B, and C) found in the deep-sea spherules, as defined in [Figure 1](#). Data from [Clayton et al. \(1986\)](#) are shown for comparison purposes for three sets of type-I deep-sea spherules (open stars), and for iron meteorite fusion crusts (black squares).

The  $\delta^{17,18}\text{O}$  values shown in [Table 2](#) do not correlate with the respective proportions of wüstite and magnetite in the ion probe spots as determined by counting pixels in digitized backscattered electron images. This lack of correlation, added to the comparable values measured for a magnetite and a wüstite/magnetite standard (see methods) demonstrate that the variations observed in  $\delta^{17,18}\text{O}$  in the cosmic spherules do not result from an instrumental artifact, i.e., a matrix effect.

Although no correlation is found between the  $\delta^{17,18}\text{O}$  values and the magnetite content on single spots, a correlation between the  $\delta^{17,18}\text{O}$  values in the spherules and the thickness of their magnetite rim is found ([Fig. 3a](#)). This suggests that this correlation exists at the scale of the whole spherule but not locally. Within the range of particle sizes analyzed in

pdfMachine

Is a pdf writer that produces quality PDF files with ease!

Produce quality PDF files in seconds and preserve the integrity of your original documents. Compatible across nearly all Windows platforms, if you can print from a windows application you can use pdfMachine.

Get yours now!

this work, the degree of heavy oxygen enrichment also correlates well with the particle diameter for the spherules of type C (Fig. 3b). The spherules with textures A and B do not show this correlation with spherule size, as their  $\delta^{18}\text{O}$  values average  $\sim 41\text{‰}$  for sizes ranging from 400 to 600  $\mu\text{m}$ .

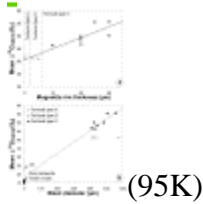


Fig. 3. (a) Correlation plot between  $\delta^{18}\text{O}$  and the thickness of magnetite rim; (b) Values of  $\delta^{18}\text{O}$  increase with the diameter of type-I deep-sea spherules belonging to textural type C (see definition of textural types in Fig. 1). Results for type A and type B spherules do not plot on this correlation. The extrapolation of this correlation line to the origin plots close to the oxygen isotopic values found in iron meteorite fusion crusts (see text).

### 3.3. Iron Isotopic Composition

Table 3 shows the iron isotopic compositions measured in nine of the eleven spherules also analyzed for oxygen. Two to four spots were analyzed for each spherule. No significant isotopic heterogeneity within individual spherules is observed. The data fall on the terrestrial fractionation line (Fig. 4) with  $\delta^{57}\text{Fe}$  values ranging from 30.3‰ to 50.2‰ (average  $\delta^{57}\text{Fe} = 43.0 \pm 7.3\text{‰}$ ) and  $\delta^{56}\text{Fe}$  values from 20.8‰ to 36.2‰ (average  $\delta^{56}\text{Fe} = 29.3 \pm 5.2\text{‰}$ ). These results are similar to those reported elsewhere (Davis et al 1991, Davis and Brownlee 1993 and Herzog et al 1999). The iron isotopic fractionation markedly increases from textural type A to textural type C.

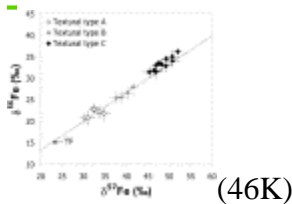


Fig. 4. Iron isotopic composition in the type-I deep-sea spherules. The data lie on a mass fractionation line. The textural types are defined in Figure 1.

### 3.4. Chromium and Nickel Isotopic Composition

Table 4 shows the isotopic compositions of chromium and of nickel in type-I spherules. As with iron, the isotopic data for chromium and nickel are consistent with mass-dependent fractionation of material that initially had terrestrial-like isotopic abundances.

Table 4.

Chromium isotopic composition measured by TIMS and nickel isotopic composition measured by ICP-MS of type-I and type-S cosmic spherules. Error limits are  $2\sigma$ .

Sample	$\delta^{50}\text{Cr}$	$\delta^{53}\text{Cr}$	$\delta^{54}\text{Cr}$	$\delta^{60}\text{Ni}$	$\delta^{61}\text{Ni}$	$\delta^{62}\text{Ni}$	$\delta^{64}\text{Ni}$
<i>type-I</i>							

Sample	$\delta^{50}\text{Cr}$	$\delta^{53}\text{Cr}$	$\delta^{54}\text{Cr}$	$\delta^{60}\text{Ni}$	$\delta^{61}\text{Ni}$	$\delta^{62}\text{Ni}$	$\delta^{64}\text{Ni}$
KK2-97A-1				71 ± 1 0	110 ± 2 6	145 ± 1 1	
KK2-97A-2	-48.3 ± 5. 8	23.6 ± 2. 8	42.8 ± 8. 5	16 ± 7	29 ± 7	32 ± 12	
KK2-97A-3				44 ± 6	63 ± 6	85 ± 9	140 ± 4 0
KK2-97A-4	-56.0 ± 5. 8	28.1 ± 2. 8	56.1 ± 5. 5	95 ± 3	123 ± 3 9	174 ± 1 0	
KK2-97A-5	-51.6 ± 5. 8	26.1 ± 2. 8	52.4 ± 5. 5	45 ± 8	45 ± 33	71 ± 18	
KK2-97A-6	-34.7 ± 5. 8	17.6 ± 2. 8	34.9 ± 5. 5	25 ± 4	35 ± 12	45 ± 9	
KK2-97A-7	-52.3 ± 5. 8	26.2 ± 2. 8	52.5 ± 5. 5	28 ± 1 0	38 ± 25	56 ± 9	
KK2-97A-8	-44.5 ± 5. 8	22.4 ± 2. 8	44.4 ± 5. 5	9 ± 5	21 ± 12	23 ± 11	
KK2-97A-9	-47.2 ± 5. 8	23.7 ± 2. 8	48.1 ± 5. 5	93 ± 6	124 ± 1 5	166 ± 1 0	
KK2-97A-10	-32.4 ± 5. 8	16.0 ± 2. 8	32.1 ± 5. 5	20 ± 4	32 ± 24	42 ± 3	85 ± 30
KK2-97A-11	-37.7 ± 5. 8	18.9 ± 2. 8	38.1 ± 5. 5	61 ± 8	97 ± 28	126 ± 1 0	
KK1-9				41 ± 1 2	62 ± 9	80 ± 12	
KK1-9*				37	61	72	
Type-S							
S12	-13.7 ± 1. 8	6.6 ± 1.0	13.4 ± 2. 0				
S13	-23.3 ± 1. 8	11.2 ± 1. 0	22.0 ± 2. 0				

\* [Herzog et al. \(1999\)](#)

-

pdfMachine

Is a pdf writer that produces quality PDF files with ease!

Produce quality PDF files in seconds and preserve the integrity of your original documents. Compatible across nearly all Windows platforms, if you can print from a windows application you can use pdfMachine.

Get yours now!

### 3.5. $\Phi$ , a Measure of Overall Mass-Dependent Fractionation

When all the isotopic data for an element fall on a single mass-dependent fractionation line, as our data do, it is convenient to have one measure of the fractionation. For this measure we adopt the slope,  $\Phi$ , of a plot of  $\delta$  values vs. the corresponding isotope mass differences for each isotopic system. We calculate the slope from our data by using the weighted least squares fitting routine of [Williamson \(1968\)](#). Qualitatively, larger  $\Phi$  means a larger degree of mass-dependent fractionation.

Values of  $\Phi$  (‰/amu) for the type-I spherules appear in [Table 5](#). We have made two different calculations of  $\Phi$  for oxygen: (1) to ease the comparison with other data, we calculate  $\Phi_{O(SMOW)}$  using the classical SMOW value as a reference ( $\delta^{18}O_{SMOW}(SMOW) = \delta^{17}O_{SMOW}(SMOW) = 0$  by definition); (2) we use the air isotopic composition ( $\delta^{18}O_{SMOW}(AIR) = 23.5\text{‰}$ ;  $\delta^{17}O_{SMOW}(AIR) = 11.8\text{‰}$ ) ([Thiemens et al., 1995](#)) as the starting isotopic composition to calculate  $\Phi_{O(AIR)}$ . The results calculated with air as the starting isotopic value are thus smaller by  $\sim 12$  ‰/amu than those calculated relative to SMOW. Because the spherule precursors interacted with atmospheric oxygen, we prefer to adopt “air” as the reference value, hence  $\Phi_{O(AIR)}$  only represents the overall mass-dependent fractionation relative to air and does not reflect the difference in isotopic composition between atmospheric oxygen and SMOW. For the type-I spherules, the average for  $\Phi_{O(AIR)}$  is  $11.6 \pm 2.7\text{‰/amu}$ , with values for individual spherules ranging from 8.4 to 15.8‰/amu.

-Table 5.

Average mass-dependent fractionation ( $\Phi$ , ‰/amu)<sup>\*</sup>, and fraction of element lost<sup>‡</sup> in type-I and type-S cosmic spherules.

Sample	$\Phi$					$f_{lost}$				
	$O_{(SMOW)}^{\text{‡}}$	$O_{(AIR)}^{\text{†}}$	Cr	Fe	Ni	$O^{\text{‡}}$	$O^{\text{†}}$	Cr	Fe	Ni
<i>type-I</i>										
KK2-97A -1	$27.9 \pm 0.3$	$15.8 \pm 0.3$		$16.1 \pm 0.3$	$36.1 \pm 2.4$	0.92	0.77		0.83	0.98
KK2-97A -2	$20.3 \pm 0.3$	$8.4 \pm 0.3$	$23.5 \pm 1.8$	$10.9 \pm 0.4$	$9.1 \pm 1.7$	0.85	0.54	0.91	0.69	0.63
KK2-97A -3	$23.2 \pm 0.2$	$11.3 \pm 0.2$		$15.6 \pm 0.7$	$21.5 \pm 1.4$	0.88	0.64		0.82	0.92
KK2-97A -4	$24.9 \pm 0.3$	$12.9 \pm 0.3$	$28.1 \pm 1.6$		$46.7 \pm 1.1$	0.90	0.69	0.95		0.99
KK2-97A -5	$24.2 \pm 0.3$	$12.2 \pm 0.3$	$26.1 \pm 1.6$		$20.0 \pm 2.9$	0.89	0.68	0.93		0.90
KK2-97A -6	$20.5 \pm 0.3$	$8.6 \pm 0.3$	$17.5 \pm 1.6$	$13.8 \pm 0.5$	$11.9 \pm 1.3$	0.85	0.55	0.84	0.78	0.73
KK2-97A -7	$23.2 \pm 0.1$	$11.2 \pm 0.1$	$26.2 \pm 1.6$	$17.1 \pm 0.7$	$14.0 \pm 2.0$	0.88	0.66	0.93	0.84	0.80
KK2-97A -8	$21.2 \pm 0.3$	$9.2 \pm 0.3$	$22.3 \pm 1.6$	$10.9 \pm 0.6$	$5.3 \pm 1.7$	0.86	0.59	0.90	0.70	0.40
KK2-97A -9	$27.7 \pm 0.2$	$15.7 \pm 0.2$	$23.8 \pm 1.6$	$17.3 \pm 0.4$	$43.5 \pm 1.8$	0.92	0.77	0.92	0.85	0.99
KK2-97A -10	$20.7 \pm 0.2$	$8.8 \pm 0.2$	$16.1 \pm 1.6$	$12.7 \pm 0.7$	$10.4 \pm 0.7$	0.85	0.56	0.81	0.75	0.70

Sample	$\Phi$					$f_{\text{lost}}$				
	$\text{O}_{(\text{SMOW})}^{\text{§}}$	$\text{O}_{(\text{AIR})}^{\text{†}}$	Cr	Fe	Ni	$\text{O}^{\text{§}}$	$\text{O}^{\text{†}}$	Cr	Fe	Ni
KK2-97A -11	$25.2 \pm 0.2$	$13.1 \pm 0.2$	$19.0 \pm 1.6$	$16.1 \pm 0.7$	$31.4 \pm 2.1$	0.90	0.71	0.86	0.83	0.9
Average $\pm 1\sigma$	$23.5 \pm 2.7$	$11.6 \pm 2.7$	$22.5 \pm 4.2$	$14.5 \pm 2.5$	$22.7 \pm 14.5$	0.88	0.65	0.89	0.79	0.8
Type-S										
S12			$6.7 \pm 0.6$	$1.6 \pm 0.5$				0.51	0.17	
S13			$11.3 \pm 0.6$	$0.6 \pm 0.2$				0.69	0.07	

<sup>¶</sup> From non-linear least squares fits ([Williamson, 1968](#)) to isotopic data assuming that the initial isotopic ratios were terrestrial.

<sup>§</sup> From the Rayleigh fractionation equation.

<sup>¥</sup> Assumes starting isotopic composition is that of standard mean ocean water (SMOW).

<sup>†</sup> Assumes starting isotopic composition is atmospheric :  $\delta^{18}\text{O}_{\text{SMOW}(\text{AIR})} = 23.5\text{‰}$ ;  $\delta^{17}\text{O}_{\text{SMOW}(\text{AIR})} = 11.8\text{‰}$  ([Thiemens et al., 1995](#)).

In general, the ranges and absolute values of  $\Phi$  calculated for Cr, Fe, and Ni resemble those reported by others ([Davis and Brownlee 1993](#), [Xue et al 1995](#) and [Herzog et al 1999](#)). We confirm the tendency of  $\Phi_{\text{Ni}}$  to increase as Ni content decreases, as expected from a well mixed evaporating system of relatively uniform starting composition ([Fig. 5](#)). Two of the spherules, 4 and 9, have remarkably large values of  $\Phi_{\text{Ni}}$ , 46.7‰/amu and 43.5‰/amu, respectively, topping the previous record of 38‰/amu ([Davis and Brownlee, 1993](#)). Increases in  $\Phi$  for the three elements correlate with one another ([Fig. 6](#)), as was noted by [Herzog et al. \(1999\)](#). For chromium higher values of  $\Phi_{\text{Cr}}$  (or lower values of  $\Phi_{\text{Fe}}$ ) are observed with respect to the correlation given in [Herzog et al. \(1999\)](#). The difference may reflect a small systematic bias ( $\sim 2\text{--}3\text{‰}$ ) as the iron isotopic compositions were measured in our case by ion microprobe and not by TIMS as in [Herzog et al. \(1999\)](#). In type A spherules the deviations from the correlation  $\Phi_{\text{Cr}}$  vs.  $\Phi_{\text{Fe}}$  are especially large, which suggests that these spherules lost a large proportion of their Cr ab initio thus leading to larger degrees of fractionation of the remaining Cr (see below).

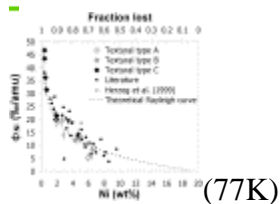


Fig. 5. Values of  $\Phi_{\text{Ni}}$ , a quantity that measures the degree of mass dependent fractionation of Ni, anticorrelate with Ni content (bottom X-axis), suggesting that the precursor particles have a limited compositional range. Literature values are from [Davis and Brownlee \(1993\)](#) and [Xue et al. \(1995\)](#). The theoretical Rayleigh distillation behavior showing the values of  $\Phi_{\text{Ni}}$  expected as a function of the retained fraction of Ni (top X-axis) is given for comparison (dotted line). Here we assume an initial Ni content of 20 wt%. The textural types are defined in [Figure 1](#).

pdfMachine

Is a pdf writer that produces quality PDF files with ease!

Produce quality PDF files in seconds and preserve the integrity of your original documents. Compatible across nearly all Windows platforms, if you can print from a windows application you can use pdfMachine.

Get yours now!

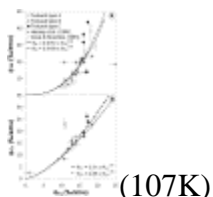


Fig. 6. Values of the quantity  $\Phi$  are correlated for the elements Fe, Cr, and Ni, in agreement with previous work (e.g., Herzog et al., 1999, and references therein). The textural types are defined in Figure 1.

#### 4. Discussion of type-I spherules

The nature of the extraterrestrial precursors of the type-I spherules is uncertain. Herzog et al. (1999) argued for small metal particles; Brownlee et al. (1997) suggested that the reduction of carbonaceous chondrite material produced metal droplets. Raisbeck et al. (1982) and Yiu et al. (1985) suggested a metal-bearing parent body for the type-I spherules, using arguments based on the unexpected presence in type-I spherules of the cosmogenic radionuclide  $^{10}\text{Be}$ . Iron meteorites contain about the same concentrations of  $^{10}\text{Be}$  as do type-I spherules, but the chemical composition of type-I spherules cannot be reconciled with that of iron meteorites (see Delaney et al., 2002).

Whatever the extraterrestrial precursors may have been, we will begin with the premise that just after melting, the type-I spherules contained no oxygen, either terrestrial or extraterrestrial, and that they evolved primarily through oxidation, and evaporation of metal and oxide, and perhaps fragmentation. As we shall see, all of the isotope data are consistent with this view.

##### 4.1. Heating Sequence: Hints from Sizes, Textures, and Compositions

The good anticorrelation between the Fe and Ni contents of all spherules (Table 1, Fig. 7) suggests a common precursor that underwent successive stages of melting and fragmentation. The thickness of the magnetite rim, as well as the abundance ratio of magnetite to wüstite, increases from textural type A to C, as do the average O, Fe and Ni isotopic fractionations. The behavior of Cr is more complex. For types B and C, the behavior of  $\Phi_{\text{Cr}}$  is compatible with that of O, Fe, and Ni. For type A, the fractionation observed is about the same as that found for type C spherules. We suggest that type A spherules lost Cr through the evaporation of a Cr-rich nugget, perhaps a sulfide, thus leading to a decreased Cr content and a larger  $\Phi_{\text{Cr}}$  in the spherule.

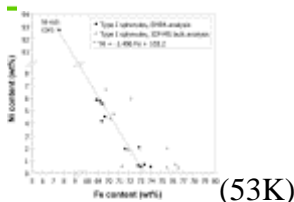


Fig. 7. Iron and nickel compositions (in wt%) of the deep-sea spherules. The solid symbols represent data obtained by averaging 2 to 5 spot analyses measured with the electron microprobe (EMPA) on the polished section. Open symbols are bulk measurements of dissolved spherules by ICP-MS. A good anticorrelation is found

between these two composition, suggesting a common precursor for the spherules, which underwent successive stages of melting and fragmentation.

The growth of magnetite rims, the ever more intimate intergrowth of magnetite and wüstite within the individual spherules, and the increasing isotopic fractionations of the major elements from type A to C spherules suggest a heating sequence, with type A heated least (lowest peak temperatures for the shortest times) and type C heated most strongly. The variations in heating intensity could be due to differences in entry speed, entry angle, or particle size. Also, Lal and Jull (2002) have suggested that an appreciable portion of the particle flux in the spherule size range comes from the atmospheric breakup of bodies larger than 1 cm. If the breakup occurred at moderate altitudes—i.e., <100 km—the resulting debris would be more strongly heated.

#### 4.2. Evaporative Losses

We will use the Rayleigh formula to calculate from  $\Phi$  (the degree of mass-dependent fractionation; Table 5) the fractions retained,  $f_r$ , of the reference isotopes  $^{16}\text{O}$ ,  $^{52}\text{Cr}$ ,  $^{54}\text{Fe}$ , and  $^{58}\text{Ni}$  after evaporation:

$$\frac{R}{R_o} = f_r^{\left(\frac{1}{\alpha}-1\right)}, \quad (1)$$

where  $R$  is an isotopic ratio,  $^{18}\text{O}/^{16}\text{O}$  for instance for oxygen, and  $R_o$  is the starting value of this ratio before evaporation and  $\alpha$  is the conventional isotopic fractionation factor. In an ideal system,

$$\alpha = \sqrt{\frac{m'}{m}} \quad (1a)$$

where  $m$  and  $m'$  are the isotopic masses of the evaporating species. Then

$$f_r = \left(1 + \frac{\Phi}{1000}\right)^b \quad (1b)$$

The exponent  $b$  is related to the conventional fractionation factor  $\alpha$  by the expression:

$$b = \frac{\alpha}{1 - \alpha} \quad (1c)$$

The relative uniformity (within 10% relative; section 3.2) of isotopic composition within a spherule shows that the oxygen in type-I spherules meets at least one of the requirements for a Rayleigh evaporation, namely, that the melts be well-mixed. As our systems may not be ideal in all respects, the choice of  $m$  requires further discussion. For the metals, Cr, Fe, and Ni, we adopt for  $m$  the masses of the isotopes themselves, e.g.,  $m = 57.94$  for  $^{58}\text{Ni}$ . In the case of nickel, this choice seems straightforward. As the most noble of the three metals, nickel oxidizes last, and, indeed, appreciable amounts of metallic Ni remain in many type-I spherules. As metallic nickel is more volatile than the oxide and as it persists through the late stages of evaporation, it is plausible that the element leaves the spherules mainly as the atom. Iron and chromium, on the other hand, are more likely to oxidize completely during descent through the atmosphere and the

nature of the evaporating species is not obvious. [Wang et al. \(1994\)](#) studied the evaporation of wüstite in the laboratory and found that use of the atomic mass of iron in Eqn. (1a) described the observations, possibly because the oxide decomposes before evaporation. Lacking experimental data for Cr, we simply assume that we can use the atomic mass of  $^{52}\text{Cr}$ . In the case of oxygen, which is bound mainly to iron, we again follow [Wang et al. \(1994\)](#), who determined fractionation factors  $\alpha = 1.0110$  and  $1.0217$  for  $^{17}\text{O}$  and  $^{18}\text{O}$ , respectively, corresponding to effective masses (amu) of 45.206 and 45.588, evaporating from wüstite for  $^{17}\text{O}$  and  $^{18}\text{O}$ , respectively.

#### 4.3. Evaporation Sequence in Type I Spherules

[Figure 8](#) and [Table 5](#) give the calculated fractions of O, Cr, Fe, and Ni lost,  $1 - f_r$ , by our type-I spherules, taking terrestrial ratios as the starting isotopic composition before evaporation. [Herzog et al. \(1999\)](#) noted that for lower degrees of evaporation—say  $\Phi_{\text{Fe}} < 5\%$ /amu and  $1 - f_{r(\text{Fe})} < 0.43$ —evaporative losses occur in the order: Fe > Cr > Ni > O (see [Fig. 6](#) and [Fig. 8](#)). If the spherules first formed as metallic droplets, then the order of loss, Fe > Ni, is the one expected based on vapor pressures of the elements ([Davis and Brownlee 1993](#) and [Herzog et al 1999](#)). The inversion of Fe and Cr may result from experimental error or early loss of Cr (see above comment regarding sulfide).

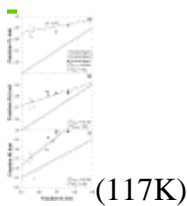


Fig. 8. Fractional evaporative losses of Cr, Fe, Ni, and O from I-type spherules. Starting isotopic compositions at the beginning of oxygen evaporation (subscript “start”) for this figure are taken as terrestrial (i.e.,  $\delta^{18}\text{O} = 23.5\%$ ,  $\delta^{17}\text{O} = 11.8\%$ ,  $\delta^x\text{Fe,Cr,Ni} = 0\%$ ). The slope one line (solid) and best linear fit lines through the data (dashed) are given for reference. The best linear fits have the following forms:  $1 - f_{r(\text{Cr})} = (0.41 \pm 0.20) \times (1 - f_{r(\text{O})}) + (0.62 \pm 0.13)$ ;  $1 - f_{r(\text{Fe})} = (0.43 \pm 0.23) \times (1 - f_{r(\text{O})}) + (0.53 \pm 0.15)$ ;  $1 - f_{r(\text{Ni})} = (1.7 \pm 0.5) \times (1 - f_{r(\text{O})}) + (-0.30 \pm 0.34)$ . The textural types are defined in [Figure 1](#).

The first stages of evaporation and isotopic fractionation of the spherules almost certainly take place before much oxygen has had a chance to react. It follows that oxygen can only begin to fractionate and “catch up” isotopically with the metals somewhat later in the evaporation process—after the oxygen reacts with the descending droplet and the loss rates of the more volatile metals have slowed. Thus it is not surprising that for spherules that have lost up to 75% of their Fe, the losses of Cr, Fe, and Ni exceed those of O. For the more strongly heated spherules, the observed order of loss shifts to Ni > Cr  $\geq$  Fe  $\sim$  O. [Figure 8](#) shows oxygen “catching up” with iron and chromium in the spherules that have larger degrees of evaporative loss. Meanwhile, the fractionation (and implied loss) of oxygen stays behind that of nickel. We interpret these observations as follows. As oxygen strikes the descending droplets, minimization of free energy first favors reaction with Cr. With the formation of the oxides of Cr, the evaporation rate of Cr decreases and, depending on the volatility of the various oxides, fractionation continues, but probably more slowly. Although the details for Cr are unclear, the concentrations of Cr are too low to have much influence on the total oxygen budget.

Once Cr has oxidized, the major element iron should oxidize next. As argued by [Davis and Brownlee \(1993\)](#), the oxidation of Fe should lower its volatility while nickel should continue to evaporate at a more or less constant rate for as long as it remains a metal (assuming constant temperature and ignoring nonideal behavior). In other words, during the latter stages of evaporation, the loss rates of iron and oxygen should approach one another but lag behind that of nickel, for as long as nickel remains unoxidized. Using the  $\Phi_{Cr}$ ,  $\Phi_{Fe}$  and  $\Phi_{Ni}$  values given in [Table 5](#), we can calculate preloss Cr/Fe of  $(3.4 \pm 1.6) \times 10^{-3}$  and Fe/Ni of  $(16.6 \pm 4.3)$  mass/mass ratios which are in good agreement with the data previously reported by others (e.g., [Herzog et al., 1999](#)).

#### 4.4. Evaporation of Fe and FeO

Here we consider the degree to which iron evaporates as metal and as oxide. We conjecture that when evaporation of the oxide begins, the iron has a single, characteristic isotopic composition and explore various values for it and their implications.

##### 4.4.1. Case 1: If the oxygen entering the spherules has $\delta^{18}O_{SMOW} = 23.5\%$ , i.e., is atmospheric, then evaporation of FeO dominates after 40% of the Fe has evaporated as metallic Fe

We take the oxygen isotopic composition to be atmospheric ( $\delta^{18}O_{SMOW(AIR)} = 23.5\%$  ([Thiemens et al., 1995](#))). If we recalculate from Eqn. (1b) the losses of Fe (as FeO) relative to a fractionated isotopic composition of iron, those losses should equal the losses calculated for oxygen. By using least squares fitting we find that by decreasing  $\Phi_{Fe}$  by  $(4.5 \pm 0.5)\%/amu$  for all samples, we obtain a fairly good match between the fractions of O and Fe lost ([Fig. 9a](#)). Because, to a good approximation, a change in the starting isotopic composition of Fe simply shifts all the measured values of  $\Phi_{Fe}$  by a fixed amount, we can say equivalently that the evaporation of O with FeO begins when the isotopic composition of iron has been fractionated by evaporation of Fe metal to the extent that  $\Phi_{Fe(start)} = (4.5 \pm 0.5)\%/amu$ , or  $\delta^{57}Fe_{start} \approx 13\%$  (the subscript “start” refers to the isotopic composition of the elements (O, Fe, Cr, Ni) when *oxygen* starts to evaporate). Application of the Rayleigh equation then shows that oxidation of iron is complete and FeO evaporation begins when  $\approx 40\%$  of the metallic Fe has evaporated. The correlation between  $\Phi_{Fe}$  and  $\Phi_{Ni}$  ([Fig. 6](#)) implies that at this point, only  $\approx 10\%$  of the Ni has evaporated. The calculated preloss Cr/Fe and Fe/Ni ratios are not affected by this hypothesis and remain as quoted above.

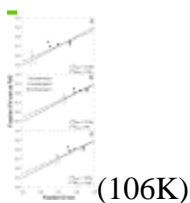


Fig. 9. The isotopic data help constrain how much Fe evaporates as metal before it oxidizes and evaporates as an oxide. The calculation rests on the requirement that after oxidation, any evaporative losses of metal and oxygen must lead to identical degrees of mass-dependent fractionation. In our calculations, the isotopic composition of both elements before evaporation are allowed to vary (see text). (a) Given a terrestrial oxygen isotopic composition equal to that measured by [Thiemens et al., 1995](#) ( $\delta^{18}O = 23.5\%$ ,  $\delta^{17}O = 11.8\%$ ), fractional losses of iron and oxygen can be made approximately equal by calculating iron losses relative to a mass-fractionated (nonterrestrial) isotopic

composition of iron that corresponds to the loss of  $\sim 40\%$  of the iron originally present; (b) fractional losses of iron and oxygen can also be made equal by considering a terrestrial starting value for iron and a “virtual” starting oxygen isotopic composition of  $\delta^{18}\text{O} = 12.5\text{‰}$ ; (c) with a starting oxygen isotopic composition of  $\delta^{18}\text{O} = 15.5\text{‰}$ , as observed by [Clayton et al. \(1986\)](#) in iron meteorite fusion crusts, a best match between the fractional iron and oxygen losses is achieved by calculating iron losses relative to a mass-fractionated isotopic composition of iron  $\Phi_{\text{Fe}(\text{start})} \sim 1.2\text{‰/amu}$ , that corresponds to the loss of  $\sim 12\%$  of the iron originally present before oxidation and subsequent evaporation of the oxide. The textural types are defined in [Figure 1](#).

#### 4.4.2. Case 2: If no Fe evaporates as metal, but only as FeO, then the oxygen entering the spherules should have $\delta^{18}\text{O}_{\text{SMOW}(\text{start})} = 12.5\text{‰}$

For completeness, we consider the case where Fe evaporates not as metal but as an oxide with  $\Phi_{\text{Fe}(\text{start})} = 0$ . We now show that a good match between  $f_{\text{O}}$  and  $f_{\text{Fe}}$  can be obtained by adopting an initial oxygen isotopic composition such that  $\Phi_{\text{O}(\text{SMOW})\text{start}} \sim 6.3\text{‰/amu}$ , or equivalently,  $\delta^{18}\text{O}_{\text{SMOW}(\text{start})} = 12.5\text{‰}$  ([Fig. 9b](#)). Choosing a reference state of oxygen different from air might seem to be an ad hoc assumption. [Clayton et al. \(1986\)](#), however, have found oxygen isotopic compositions in iron meteorite fusion crusts with  $\delta^{18}\text{O}_{\text{SMOW}} \sim 15.5\text{‰}$ , which is  $\sim 8\text{‰}$  lower than that of air ( $\delta^{18}\text{O}_{\text{SMOW}(\text{AIR})} = 23.5\text{‰}$ , [Thiemens et al., 1995](#)). As the oxygen present in these fusion crusts comes from oxidation of incoming meteoritic metal during atmospheric entry, [Clayton et al. \(1986\)](#) concluded that a kinetic isotope effect took place during oxidation of iron. The iron meteorites thus acquired oxygen from the atmosphere with a fractionation of approximately  $-8\text{‰}$  in  $\delta^{18}\text{O}$ .

#### 4.4.3. Case 3: If the oxygen entering the spherules has $\delta^{18}\text{O}_{\text{SMOW}(\text{start})} = 15.5\text{‰}$ , the same value as fusion crusts in iron meteorites, then evaporation of FeO dominates after 12% of the Fe has evaporated as metallic Fe

If we take  $\delta^{18}\text{O}_{\text{SMOW}} \sim 15.5\text{‰}$  as the starting oxygen isotopic composition before evaporation (see above or [Clayton et al., 1986](#)), then a best fit between the fractions of O and Fe lost is obtained with an initial  $\delta^{57}\text{Fe} = 3.5\text{‰}$ , or  $\Phi_{\text{Fe}(\text{start})} \sim 1.2\text{‰/amu}$  ([Fig. 9c](#)), which means that  $\sim 12\%$  of the iron evaporated as metal before oxidizing and evaporating (more slowly) as oxide. The correlation between  $\Phi_{\text{Fe}}$  and  $\Phi_{\text{Ni}}$  ([Fig. 6](#)) implies that at this point, less than a few percent of Ni has evaporated.

In summary, we conclude that the oxygen isotopic composition of the oxygen entering the spherules—the “apparent atmospheric composition”—must be between  $\delta^{18}\text{O} = 12.5\text{‰}$  and  $23.5\text{‰}$ . The corresponding amounts of evaporation of metallic iron before oxidation are between 39 and 0%, respectively. Case 2 does not seem realistic, as evaporation of iron was most probably competing with the oxidation process. Case 1 and 3 seem equally probable, but we rely on the measurements of the oxygen isotopic compositions of iron meteorite fusion crusts by [Clayton et al. \(1986\)](#) to favor case 3. In that case  $\sim 12\%$  of iron evaporated as metal before oxidation became essentially complete. The “apparent” oxygen isotopic composition of the atmosphere is that case is  $\delta^{18}\text{O}_{\text{SMOW}} \sim 15.5\text{‰}$ , with  $\delta^{17}\text{O}_{\text{SMOW}} \sim 8\text{‰}$ .

With this starting oxygen isotopic composition, one can also calculate a best match between the loss of oxygen and that of  $\text{Cr}_2\text{O}_3$ . It is obtained for a starting  $\Phi_{\text{Cr}(\text{start})} \sim 12\text{‰/amu}$ , which means that  $\sim 70\%$  of the Cr evaporated as metal (more if the

evaporating entity was a heavier sulfide) before loss as oxide (Fig. 10a). The quality of this fit is not as good as with Fe. This might be due to the relatively small amount of Cr available and the associated analytical uncertainty. The behavior of Cr is perhaps also more complex than this two-step mechanism suggests, and the Rayleigh hypothesis of a perfect instantaneous mixing may not be realized during the early states of evaporation.

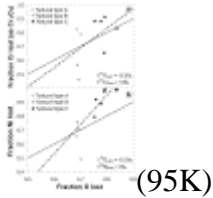


Fig. 10. (a) The isotopic data for Cr constrain how much Cr evaporates as metal before it oxidizes and evaporates as an oxide. With a starting oxygen isotopic composition on the terrestrial fractionation line with  $\delta^{18}\text{O} = 15.5\text{‰}$  (see Fig. 9) the average fractional losses of chromium and oxygen can be made approximately equal by calculating chromium losses relative to a mass-fractionated isotopic composition ( $\Phi_{\text{Cr}(\text{start})} = 12\text{‰/amu}$ ). However Cr as a very minor element does not control the oxygen budget. The apparent good fit observed here can be explained by the similarity between the observed values of  $\Phi_{\text{Fe}}$  and  $\Phi_{\text{Cr}}$ . (b) By proceeding as in Figure 10a, it is impossible to reconcile the losses of nickel, as calculated from its isotopic composition with those of oxygen. Nickel was probably mostly lost as metal, and not as oxide. The textural types are defined in Figure 1.

It is not possible to reconcile the losses of O and Ni by using the methods described above for Fe. In most cases, Ni probably evaporated too fast as metal for it to have had time to oxidize in significant amounts. Figure 10b shows the fractional losses of O and Ni with the starting oxygen isotopic composition of  $\delta^{18}\text{O} = 15.5\text{‰}$ .

#### 4.5. Rarity of Spherules with Little Mass-Dependent Fractionation of Cr and Fe

Type-I spherules with little mass-dependent fractionation are of special interest because their compositions should resemble most closely those of the precursor material. Curiously, only 2 of 24 and 2 of 14 type-I spherules, respectively, have values of  $\Phi_{\text{Fe}}$  and  $\Phi_{\text{Cr}}$  less than 10‰/amu, a value that already corresponds to substantial elemental losses,  $\sim 60\%$ . For Ni, the fraction of objects with little mass-dependent fractionation is larger: low values of  $\Phi_{\text{Ni}}$ , < 10‰/amu, occur in 9 of 43 spherules (this work, and Herzog et al., 1999, and references therein). We infer that once melting has taken place, evaporation of iron proceeds very quickly relative to the total time available for evaporation, 5–20 s (Yada et al., 1996). An alternative explanation, that subaerial weathering destroys objects that retain more metal, seems unlikely for the corrosion-resistant, Ni-rich spherules. Conceivably only those type-I spherules that are specially armored in some unknown way by atmospheric heating survive for long in ocean sediments. A detailed, systematic study of the surfaces of type-I spherules, which vary considerably (e.g., Czajkowski, 1987) might prove worthwhile.

### 5. Results of stony (type S) Cosmic spherules

#### 5.1. Sizes, Textures, and Chemical Compositions

Table 6 summarizes the sizes, textures, and chemical compositions of all stony spherules except S12 and S13. The apparent diameters of thirteen Antarctic S-type spherules range

from  $\sim 100 \mu\text{m}$  to  $\sim 200 \mu\text{m}$ ; the deep-sea particle is larger, with a diameter of  $\sim 400 \mu\text{m}$ . Three spherules are of the barred olivine type (BO; e.g., Fig. 11a), one consists of radial pyroxene (RP; Fig. 11b), and one looks like a glass spherule (Gl; Fig. 11c). The remaining nine stony spherules are porphyritic olivine (PO; e.g., Fig. 11d) with two of them being very fine-grained (94-4-14 and 94-4B-45), and four of them only partially melted with relict grains (94-4-14B, 94-4B-6, 94-4B-12 and 94-4B-43, e.g., Figs. 11e and 11f).

Table 6.

Chemical composition (wt%) of 13 stony cosmic spherules from Antarctica (94-4 and 94-4B series) and one stony deep sea spherule (KK2-97A-23) measured by electron microprobe at the location of the ion microprobe spots. The data are arranged by textural type.

Sample	D* ( $\mu\text{m}$ )	Type	Phase s analy zed <sup>†</sup>	O	Na	Mg	Al	Si	P	S	K	Ca	Ti	Cr	Mn	Fe	Ni	Total
94-4-11_1	195	BO	Ol + Gl + Mt	36.5	0.2	1.8	0.7	1.9	b.d.	0.4	b.d.	0.9	0.8	0.1	0.5	3.4	0.1	97.8
94-4-11_2	195	BO	Ol + Gl + Mt	37.0	0.2	1.5	0.6	1.6	b.d.	0.2	b.d.	0.7	0.3	0.2	0.4	2.8	0.1	97.4
94-4B_42_1-3	150	BO	Ol + Gl + Mt	38.0	0.1	1.6	1.4	1.5	0.4	b.d.	0.2	1.8	0.6	0.0	0.9	2.7	0.8	99.8
KK297A-23_1-4	400	BO	Ol + Gl + Mt	42.3	b.d.	1.8	1.4	2.5	n.a.	n.a.	n.a.	0.6	0.6	0.7	0.3	1.7	0.9	101.08
94-4B-25_1,2	135	Gl	Gl	43.1	b.d.	1.7	1.8	2.3	n.a.	n.a.	n.a.	2.1	0.1	0.3	0.1	9.3	0.1	97.2
94-4-32_1	140	RP	Px + Plag	38.3	0.6	1.4	1.4	1.7	0.1	0.4	0.8	1.5	0.1	0.7	0.3	2.1	0.6	96.3
94-4-32_2	140	RP	Px + Plag	38.5	0.5	1.4	1.7	1.7	0.8	0.3	0.6	1.4	0.7	0.2	0.5	2.5	0.8	97.7
94-4-32_3	144	RP	Px + Plag	38.4	0.4	1.4	1.5	1.6	0.1	0.1	0.1	1.4	0.4	0.4	0.3	2.2	0.0	96.2

Sample	D* (µm)	Type	Phase analyzed	O	Na	Mg	Al	Si	P	S	K	Ca	Ti	Cr	Mn	Fe	Ni	Total
	0			0	6	4	5	9	7	8	7	6	7	4	2	2	4	7
94-4-32_4	140	RP	Px + Plag	400	031	137	1.39	190	021	006	003	475	015	002	007	188	004	99.23
94-4-14_1	180	PO	Ol + Gl + Mt	369	b.d.	129	081	154	002	000	001	169	004	009	007	310	024	99.77
94-4-14_2	180	PO	Ol + Gl + Mt	359	004	125	1.02	141	005	0038	b.d.	177	004	003	001	314	027	98.18
94-4B-45_1,2	160	PO	Ol + Gl + Mt	401	002	178	1.17	176	008	0001	0011	100	009	004	0025	222	037	100.91
94-4B_26_1	160	PO	Ol + Gl	433	005	122	2.61	236	009	0012	0001	283	006	004	001	144	003	100.33
94-4B_26_2	160	PO	Ol + Gl	300	005	54	0.21	179	003	0013	0003	0059	0010	0062	0022	421	010	91.07
94-4-13_1	185	PO	Ol + Gl + Mt	369	001	42	3.22	178	007	0002	b.d.	474	001	002	008	300	008	97.52
94-4-13_2	185	PO	Ol + Gl + Mt	368	002	94	2.29	162	002	b.d.	b.d.	246	000	003	006	300	000	98.14
94-4-8_1	125	PO	Ol + Gl + Mt	339	b.d.	30	2.61	156	000	b.d.	001	376	001	003	003	346	012	94.44
94-4-8_2	125	PO	Ol + Gl + Mt	376	001	11	0.74	161	003	0001	b.d.	086	004	004	000	249	007	97.59

pdfMachine

Is a pdf writer that produces quality PDF files with ease!

Produce quality PDF files in seconds and preserve the integrity of your original documents. Compatible across nearly all Windows platforms, if you can print from a windows application you can use pdfMachine.

Get yours now!

Sample	D* ( $\mu$ m)	Type <sup>§</sup>	Phase s analy zed <sup>‡</sup>	O	Na	Mg	Al	Si	P	S	K	Ca	Ti	Cr	Mn	Fe	Ni	Total
94-4-14B_1	190	PO <sup>‡</sup>	Ol + Mx + Mt	40.1	0.01	21.2	0.36	1.83	0.06	0.01	0.01	0.09	0.02	0.08	0.02	1.47	0.27	96.34
94-4-14B_2	190	PO <sup>‡</sup>	Ol + Mx + Mt	39.7	b.d.	20.6	0.16	1.77	0.04	0.01	0.02	0.06	0.03	0.00	0.03	1.83	0.16	97.96
94-4B-6	140	PO <sup>‡</sup>	Ol + Mx + Mt	44.5	0.23	17.9	1.42	2.35	0.15	0.00	0.01	1.06	0.11	0.07	0.05	8.77	0.34	99.74
94-4B-12	130	PO <sup>‡</sup>	Ol + GI	43.7	0.08	17.0	1.46	2.33	0.11	0.02	0.01	1.05	0.09	0.06	0.05	1.21	0.04	100.33
94-4B-43_1	140	PO <sup>‡</sup>	Fo <sub>98.8</sub>	45.1	0.01	33.5	0.02	1.97	n.a.	n.a.	n.a.	0.12	0.03	0.06	0.03	1.00	b.d.	100.19
94-4B-43_2	140	PO <sup>‡</sup>	Fo <sub>98.7</sub> + Mx	45.5	b.d.	32.3	0.08	2.00	n.a.	n.a.	n.a.	0.06	0.01	0.03	0.00	1.00	0.02	100.60
94-4B_43_3	140	PO <sup>‡</sup>	Fo <sub>98.6</sub> + zonin g	45.2	0.01	33.6	0.02	1.96	n.a.	n.a.	n.a.	0.13	0.01	0.07	0.05	1.01	b.d.	100.66
94-4B_43_4	140	PO <sup>‡</sup>	Mx	39.4	0.08	14.0	1.28	1.77	0.12	0.03	0.05	1.09	0.07	0.07	0.02	2.61	0.19	101.13
94-4B_43_5	140	PO <sup>‡</sup>	Fo + Mx	43.0	0.03	26.9	0.07	1.83	0.05	0.05	b.d.	0.05	0.03	0.06	0.00	1.06	0.35	101.25

b.d.: below detection limit of ~0.01 wt%; n.a.: not analyzed.

\* Average diameter as measured on the polished section.

§ Textural type of cosmic spherules: BO = barred olivine; GI = Glass; RP = radial pyroxene; PO = porphyritic olivine

‡ PO = Porphyritic olivine but only partially melted.

‡ The ion microprobe beam spot included sometimes several mineral phases: Ol =

pdfMachine

Is a pdf writer that produces quality PDF files with ease!

Produce quality PDF files in seconds and preserve the integrity of your original documents. Compatible across nearly all Windows platforms, if you can print from a windows application you can use pdfMachine.

Get yours now!

olivine; Gl = glass; Mt = magnetite; Mx = matrix material; Px = pyroxene; Plag = plagioclase. The Fo numbers refer to the forsterite content (in mol%) of the olivine grains analyzed in spherule #94-4B-43.

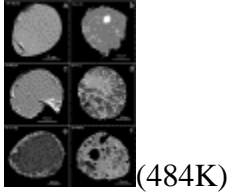


Fig. 11. Backscattered electron micrographs of polished sections of the textural types found in our sampling of type-S (stony) spherules. (a) Barred olivine (BO); (b) radial pyroxene spherule (RP) with pyroxene bars and feldspathic (plagioclase) glass. Bright spots are remnants of gold coating that was not totally removed by polishing after ion microprobe analysis. Small amounts of igneous rims are shown by white arrows; (c) Glass spherule (Gl); (d–f) porphyritic olivine spherules (PO); (d) PO spherule largely melted with a few relict forsteritic cores in the recrystallized olivine grains; (e) PO spherule with a very large unmelted core; and (f) partially melted PO spherule with relict forsteritic olivine grains.

As we do not have direct access to the bulk chemical compositions of the stony spherules, we make the assumption that the means of our electron microprobe analyses (Table 6) give reasonable proxies for these bulk compositions. In our sampling of 14 spherules, we find depleted Mg/Si and Al/Si average atomic ratios (0.95 and 0.074, respectively) compared to the corresponding average values for 68 Antarctic stony spherules of 1.06 and 0.091 given by Brownlee et al. (1997), and of 1.05 and 0.090, respectively, for 46 BO spherules analyzed by Taylor et al. (2000). The average Mg/Si and Al/Si atomic ratios calculated for our three BO spherules are 0.95 and 0.068, respectively.

The mean Ca/Si and Fe/Si atomic ratios found for our 14 spherules (0.062 and 0.61, respectively) are intermediate between the mean ratios of 0.056 and 0.53 measured by Brownlee et al. (1997) in Antarctic spherules and that of 0.073 and 0.61 reported by Taylor et al. (2000) in 46 BO spherules. In our 14 spherules, the average Mg/Si, Al/Si, and Fe/Si atomic ratios normalized to CI values (Anders and Grevesse, 1989) are slightly less than one (0.88, 0.88, and 0.68, respectively). The Ca/Si atomic ratio is chondritic (Ca/Si = 1.02 normalized to CI).

## 5.2. Oxygen Isotopic Composition

Because of the small sizes of the mineral grains, the beam of the ion microprobe sometimes included several phases (Table 7). The oxygen in the stony cosmic spherules is generally enriched in  $^{17}\text{O}$  and  $^{18}\text{O}$  relative to SMOW, although to a lesser degree than the oxygen in the type-I spherules (Table 7; Fig. 12). The values of  $\delta^{18}\text{O}$  range from  $-0.1\text{‰}$  to  $29.8\text{‰}$  and of  $\delta^{17}\text{O}$  from  $-5.0\text{‰}$  to  $13.8\text{‰}$ . The oxygen isotope enrichment broadly correlates with textural type (Fig. 12): the barred olivine (“BO”) and the totally melted porphyritic olivine (“PO melted”) spherules have the heaviest oxygen; the glass (“Gl”) and the porphyritic olivine spherules which were only partially melted (“PO part. melted”) have a low degree of heavy isotope enrichment, with variable isotopic compositions, especially for 94-4B-43 with  $1.5\text{‰} < \delta^{18}\text{O} < 24.7\text{‰}$  (Table 7); the

pdfMachine

Is a pdf writer that produces quality PDF files with ease!

Produce quality PDF files in seconds and preserve the integrity of your original documents. Compatible across nearly all Windows platforms, if you can print from a windows application you can use pdfMachine.

Get yours now!

radiating pyroxene spherule (“RP”) plots in the range of unmelted minerals in AMMs (Engrand et al., 1999). There is no correlation between the apparent sizes (or masses) of the stony cosmic spherules and their oxygen isotopic compositions.

Table 7.

*In situ* oxygen isotopic composition measured by ion microprobe in 13 stony cosmic spherules from Antarctica (94-4 and 94-4B series), and in one stony deep-sea spherule (KK297A-23). The data are arranged by textural type.

Sample	D* ( $\mu\text{m}$ )	Type <sup>§</sup>	Phases analyzed <sup>‡</sup>	$\delta^{18}\text{O} \pm \sigma$ (‰) <sup>‡</sup>	$\delta^{17}\text{O} \pm \sigma$ (‰) <sup>‡</sup>	$\Delta^{17}\text{O} \pm \sigma$ (‰) <sup>‡§</sup>
94-4-11_1	195	BO	Ol + Gl + Mt	23.9 $\pm$ 1.4	12.0 $\pm$ 1.0	-0.4 $\pm$ 1.1
94-4-11_2	195	BO	Ol + Gl + Mt	19.8 $\pm$ 1.3	9.5 $\pm$ 1.0	-0.8 $\pm$ 1.1
94-4B_42_1	150	BO	Ol + Gl + Mt	26.6 $\pm$ 2.0	9.7 $\pm$ 1.4	-4.1 $\pm$ 1.1
94-4B-42_2	150	BO	Ol + Gl + Mt	27.7 $\pm$ 1.2	9.8 $\pm$ 1.1	-4.6 $\pm$ 1.1
94-4B-42_3	150	BO	Ol + Gl + Mt	29.0 $\pm$ 1.2	11.0 $\pm$ 1.2	-4.0 $\pm$ 1.2
KK297A-23_1	400	BO	Ol + Gl + Mt	23.6 $\pm$ 1.9	13.6 $\pm$ 1.2	1.3 $\pm$ 1.0
KK297A-23_2	400	BO	Ol + Gl + Mt	22.2 $\pm$ 1.8	11.7 $\pm$ 1.0	0.2 $\pm$ 0.6
KK297A-23_3	400	BO	Ol + Gl + Mt	20.5 $\pm$ 1.8	12.0 $\pm$ 1.0	1.3 $\pm$ 0.7
KK297A-23_4	400	BO	Ol + Gl + Mt	18.4 $\pm$ 1.8	10.8 $\pm$ 1.0	1.2 $\pm$ 0.6
94-4B-25_1	135	Gl	Gl	4.9 $\pm$ 1.2	-3.4 $\pm$ 1.4	-6.0 $\pm$ 1.3
94-4B-25_2	135	Gl	Gl	3.4 $\pm$ 1.2	-3.5 $\pm$ 1.4	-5.2 $\pm$ 1.3
94-4-32_1	140	RP	Px + Plag	3.7 $\pm$ 1.3	1.7 $\pm$ 0.8	-0.2 $\pm$ 0.8
94-4-32_2	140	RP	Px + Plag	7.2 $\pm$ 1.4	3.8 $\pm$ 1.1	0.1 $\pm$ 1.1
94-4-32_3	140	RP	Px + Plag	6.6 $\pm$ 1.6	2.0 $\pm$ 1.0	-1.4 $\pm$ 1.1
94-4-32_4	140	RP	Px + Plag	7.4 $\pm$ 1.2	3.6 $\pm$ 1.1	-0.3 $\pm$ 1.1
94-4-14_1	180	PO	Ol + Gl + Mt	22.3 $\pm$ 1.2	12.1 $\pm$ 0.7	0.5 $\pm$ 0.8
94-4-14_2	180	PO	Ol + Gl + Mt	20.1 $\pm$ 1.2	10.9 $\pm$ 0.7	0.5 $\pm$ 0.7
94-4B-45_1 <sup>a</sup>	160	PO	Ol + Gl + Mt	24.2 $\pm$ 1.7	8.9 $\pm$ 1.5	-3.7 $\pm$ 1.4
94-4B-45_2	160	PO	Ol + Gl + Mt	23.4 $\pm$ 1.3	9.0 $\pm$ 1.1	-3.2 $\pm$ 1.1
94-4B_26_1 <sup>b</sup>	160	PO	Ol + Gl	14.2 $\pm$ 1.1	6.4 $\pm$ 0.9	-0.9 $\pm$ 0.7

pdfMachine

Is a pdf writer that produces quality PDF files with ease!

Produce quality PDF files in seconds and preserve the integrity of your original documents. Compatible across nearly all Windows platforms, if you can print from a windows application you can use pdfMachine.

Get yours now!

Sample	D <sup>*</sup> (μm)	Type <sup>§</sup>	Phases analyzed <sup>‡</sup>	δ <sup>18</sup> O ± σ (‰) <sup>†</sup>	δ <sup>17</sup> O ± σ (‰) <sup>†</sup>	Δ <sup>17</sup> O ± σ (‰) <sup>‡‡</sup>
94-4B_26_2 <sup>b</sup>	160	PO	Ol + Gl	18.7 ± 1.0	7.4 ± 0.8	-2.3 ± 0.7
94-4-13_1	185	PO	Ol + Gl + Mt	29.1 ± 1.4	13.8 ± 0.7	-1.4 ± 0.8
94-4-13_2	185	PO	Ol + Gl + Mt	29.8 ± 1.2	11.3 ± 0.9	-4.2 ± 0.9
94-4-8_1	125	PO	Ol + Gl + Mt	18.5 ± 1.2	10.6 ± 1.2	0.9 ± 1.2
94-4-8_2	125	PO	Ol + Gl + Mt	16.8 ± 1.3	10.6 ± 0.9	1.9 ± 0.9
94-4-14B_1	190	PO <sup>‡</sup>	Ol + Mx + Mt	8.9 ± 1.3	0.6 ± 0.8	-4.1 ± 0.9
94-4-14B_2	190	PO <sup>‡</sup>	Ol + Mx + Mt	0.7 ± 1.4	-2.9 ± 0.8	-3.2 ± 0.9
94-4B-6_1	140	PO <sup>‡</sup>	Ol + Mx	-0.1 ± 1.2	-4.2 ± 1.2	-4.1 ± 1.1
94-4B-12_1	130	PO <sup>‡</sup>	Ol + Gl	1.1 ± 1.2	-1.1 ± 1.0	-1.7 ± 0.9
94-4B-43_1	140	PO <sup>‡</sup>	Fo <sub>98.8</sub>	13.4 ± 1.4	2.9 ± 1.7	-4.0 ± 1.7
94-4B-43_2	140	PO <sup>‡</sup>	Fo <sub>98.7</sub> + Mx	1.5 ± 1.3	-5.0 ± 1.4	-5.8 ± 1.3
94-4B_43_3	140	PO <sup>‡</sup>	Fo <sub>98.6</sub> + zoning	16.8 ± 1.9	4.7 ± 1.2	-4.0 ± 0.8
94-4B_43_4	140	PO <sup>‡</sup>	Mx	24.7 ± 1.9	10.1 ± 1.2	-2.8 ± 0.8
94-4B-43_5	140	PO <sup>‡</sup>	Fo + Mx	14.5 ± 2.5	2.4 ± 1.5	-5.2 ± 1.5

\* Average diameter as measured on the polished section.

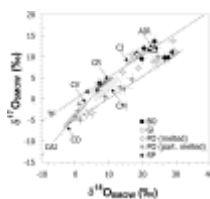
§ Textural types of cosmic spherules: BO = barred olivine; Gl = Glass; RP = radial pyroxene; PO = porphyritic olivine

‡ PO = Porphyritic olivine but only partially melted.

‡ The ion microprobe beam spot included sometimes several phases: Ol = olivine; Gl = glass; Mt = magnetite; Px = pyroxene; Plag = plagioclase; Mx = matrix. The Fo numbers refer to the forsterite content (in mol%) of the olivine grains analyzed in spherule #94-4B-43. <sup>a,b</sup>Weighted mean of two and three analyses on the same spot, respectively.

† Relative to SMOW, errors are 1σ mean.

‡ Δ<sup>17</sup>O ≈ δ<sup>17</sup>O - 0.52 × δ<sup>18</sup>O.



(59K)

pdfMachine

Is a pdf writer that produces quality PDF files with ease!

Produce quality PDF files in seconds and preserve the integrity of your original documents. Compatible across nearly all Windows platforms, if you can print from a windows application you can use pdfMachine.

Get yours now!

Fig. 12. Oxygen isotopic compositions of individual type-S spherules calculated relative to standard mean ocean water (SMOW). The solid line labeled TF is the terrestrial fractionation line anchored at SMOW and calculated from the relations

$$\delta(^{17,18}\text{O}) = \left( f_{\text{retained}}(^{16}\text{O}) \right)^{\alpha-1} - 1 \times 1000, \text{ where } \alpha = \sqrt{\frac{m(^{16}\text{O})}{m(^{17,18}\text{O})}}$$

and  $f_{\text{retained}}$  is allowed to vary from 0.1 to 1.7; values of  $f_{\text{retained}}$  greater than 1.0 correspond physically to mass gains from condensation. To a good approximation,  $\delta^{17}\text{O} = 0.52 \times \delta^{18}\text{O}$ . The line labeled CAI was read from Figure 2 of Clayton (1993); it has the form  $\delta^{17}\text{O} = 0.938 \times \delta^{18}\text{O} - 4.06$ . The slope 0.52 short dotted line represents the range of variation expected (relative to SMOW) in samples that underwent mass-dependent fractionation. Data for CI, CM, CR, and CO chondrites represent whole-rock analyses of meteorite falls taken from Rowe et al 1994, Weisberg et al 1993 and Bischoff et al 1993, and Clayton and Mayeda 1984, Clayton and Mayeda 1999 and Clayton and Mayeda 2001). Most data for minerals from unmelted Antarctic meteorites lie between the TF and the CAI line with a lowest value of  $\delta^{18}\text{O} = -11.3\text{‰}$  for non-refractory minerals (Engrand et al., 1999).

### 5.3. Variability of Oxygen Isotope Composition within Spherules

In particle 94-4B-43, a porphyritic spherule with an apparent radius of 140  $\mu\text{m}$ , the values of  $\delta^{18}\text{O}$  range from 1.5‰ to 24.7‰, thus covering most of the spread established by the other 13 samples (Table 7, Fig. 13). This large variability may be due to the presence of unmelted, relict grains. The  $\delta^{18}\text{O}$  variability within the other type-S spherules with two or more measurements is considerably smaller, only  $(3.2 \pm 2.3)\text{‰}$  on average. This spread is roughly comparable to the ranges observed in individual type-I spherules, and is consistent with variability expected given the measurement error on any one spot. Only one other particle, the porphyritic spherule 94-4-14B, has a range in  $\delta^{18}\text{O}$  greater than 6‰. We might expect smaller spreads in the range of oxygen isotopic values in the more strongly heated samples but the average for the barred olivine spherules  $(3.9 \pm 1.5)\text{‰}$  is not significantly different from the average for the entire set; moreover, in two of the barred olivine spherules,  $\delta^{18}\text{O}$  varies by  $\sim 4\text{‰}$ . We conclude that most of the particle melts were generally isotopically homogeneous.

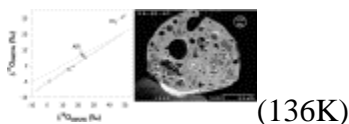


Fig. 13. Oxygen three isotope diagram of the porphyritic olivine partially melted spherule 94-4B-43. This spherule exhibits a range of variation in  $\delta^{18}\text{O}$  values of more than 20‰. Two olivine grains with about the same composition ( $\text{Fo}_{98.7}$  and  $\text{Fo}_{98.8}$ ) have  $\delta^{18}\text{O}$  values that differ by more than 10‰. A best fit through the data gives a linear equation:  $y = 0.645x - 6.1273$ , with  $R^2 = 0.992$ . The values for atmospheric air and atmospheric  $\text{CO}_2$  at 60 km altitude are given for reference (Thiemens et al., 1995). The backscattered electron micrograph of this spherule is given on the right where the analysis areas (ellipses) are labeled with their corresponding  $\delta^{18}\text{O}$  values.

pdfMachine

Is a pdf writer that produces quality PDF files with ease!

Produce quality PDF files in seconds and preserve the integrity of your original documents. Compatible across nearly all Windows platforms, if you can print from a windows application you can use pdfMachine.

Get yours now!

#### 5.4. Isotopic Composition of Fe and Cr in Two Type-S Spherules

[Table 3](#) and [Table 4](#) include the Cr and Fe isotopic compositions of two type-S deep-sea spherules of unknown petrographic type. The fractionation of iron is small for both spherules ( $1.6 \pm 0.5$ )‰/amu for S12 and ( $0.6 \pm 0.2$ )‰/amu for S13 consistent with the generally small values of  $\delta^{57}\text{Fe}$  reported by [Taylor et al. \(2002\)](#) for other S-type spherules. In both instances the fractionation of Cr isotopes is larger, ( $6.7 \pm 0.6$ )‰/amu for S12 and ( $11.3 \pm 0.6$ )‰/amu for S13, although not in any simple relation to the fractionation of Fe. We conclude that most of the particle melts were relatively well mixed, i.e., homogeneous on a scale of a few microns or more.

### 6. Discussion of type-S spherules

#### 6.1. Comparison with Other Oxygen Isotope Data

[Clayton et al. \(1986\)](#) analyzed four pooled samples of stony cosmic spherules from the deep-sea (KK1) collection; the samples contained from 42 to 315 particles each. The average values of  $\delta^{18}\text{O}$  and  $\delta^{17}\text{O}$  relative to SMOW for the four sets were ( $24 \pm 1$ )‰ and ( $10 \pm 1$ )‰, respectively. Each of these four measurements was effectively weighted by the cube of the average particle radius, which varied in the four splits. Even so, intersample variations of the oxygen isotopic abundances of the pooled samples are small, suggesting a weak dependence on particle radius.

For the 13 Antarctic and 1 deep-sea stony (type-S) spherules analyzed here, the measured values of  $\delta^{18}\text{O}$  and  $\delta^{17}\text{O}$  average, respectively, ( $16 \pm 9$ )‰ and ( $6 \pm 6$ )‰ relative to SMOW ([Table 7](#) and [Fig. 12](#)). The large standard deviations of these averages reflect a spread in the data much larger than the uncertainties of the individual measurements (estimated to be  $\sim 1$ ‰) and reaffirm the particle-to-particle variability evident in [Figure 12](#). The oxygen data therefore indicate that our set of samples differs in a systematic way from the set (KK1) analyzed by [Clayton et al. \(1986\)](#). As now discussed, we believe that collection bias explains the difference.

[Taylor et al. \(2000\)](#) have compared the populations of particle types found in deep-sea (KK1) and in Antarctic surface collections. In the deep-sea collection, barred olivine and type-I spherules dominate, accounting for  $\sim 50$  and 25% of all extraterrestrial particles. If we exclude the type-I particles, the percentage of barred olivine spherules in the deep-sea collection rises to 67%. Cryptocrystalline and glass particles make up less than 3% of the deep-sea total. In contrast, in the Antarctic surface collection, cryptocrystalline and glass particles occur in much greater abundance, 18%, as do relict grains and porphyritic and barred olivine spherules ([Taylor et al., 2000](#)). Under the circumstances, it makes more sense to compare the oxygen isotope abundances measured by [Clayton et al. \(1986\)](#),  $\delta^{18}\text{O} = 24$ ‰ and  $\delta^{17}\text{O} = 10$ ‰, with the average that we obtained for 3 barred olivine spherules,  $\delta^{18}\text{O}(\text{‰}) = 24 \pm 4$  and  $\delta^{17}\text{O}(\text{‰}) = 11 \pm 1$ . The better agreement observed between these two sets of data suggests that the relatively large  $\delta^{18,17}\text{O}$  values reported by [Clayton et al. \(1986\)](#) reflect the underrepresentation in the deep-sea collection of porphyritic, cryptocrystalline and glass particles, which were presumably destroyed by weathering. At the same time, the overall agreement for the barred olivine particles should not disguise the importance of the interparticle variability that we observe, a point discussed further in [section 6](#).

[Yada et al 2002](#), [Yada et al 2003a](#), [Yada et al 2003b](#) and [Yada et al 2003c](#) have recently reported ion microprobe oxygen isotopic analyses of Antarctic cosmic spherules from the

Japanese collection. For the 36 stony spherules they analyzed, ~75% of the data plot on or close to the terrestrial fractionation line within analytical errors, with  $\delta^{18}\text{O}$  values from ~0‰ to ~50‰, and  $\delta^{17}\text{O}$  values ranging from ~1‰ to ~30‰. Two extreme values are found, one at  $\delta^{18}\text{O} = 93\%$  slightly below the TF line, and the other with  $\delta^{18}\text{O} \sim 50\%$  and  $\Delta^{17}\text{O} = +13\%$ . [Yada et al 2002](#), [Yada et al 2003a](#) and [Yada et al 2003b](#)) interpret most of the data as resulting from large mass dependent fractionation due to evaporation of a large fraction of the grains.

## 6.2. Possible Mechanisms for Setting O Isotope Composition of Spherules

The isotopic data for oxygen are considered within the context of three possible mechanisms for setting their isotope composition. First, the spherules may have variable initial (pre-atmospheric entry) compositions, as is observed in whole-rock carbonaceous chondrites (e.g., [Clayton and Mayeda, 1999](#)). For example, some particles may have initially resembled CM chondrites and some CI chondrites (e.g., [Kurat et al 1994](#) and [Enggrand and Maurette 1998](#)), or even some composition not represented in the current collection of meteorites. Second, the particles undoubtedly underwent some mass loss during atmospheric entry, and their isotopic compositions may have been fractionated during this event. Third, the particles may have exchanged isotopes with oxygen in the atmosphere. It is likely that the spherules record all three processes to varying degrees. To assess the importance of these processes, the data of [Figure 12](#) are replotted in [Figure 14](#) ([Table 8](#)) as particle weighted means with range bars (excluding the one clearly heterogeneous particle 94-4B-43, which is discussed later). From [Figure 14](#), we can define two main groups of particles: (1) the barred-olivine (BO) and the totally melted porphyritic olivine spherules (PO melted) have oxygen isotopic values that lie close to, but in many cases are slightly isotopically heavier than the field of CI chondrites and are also compatible with the values found for air; and (2) the types GI, RP, and PO partially melted spherules scatter along the CAI line, and close to established fields for bulk CR, CM or CO chondrites.

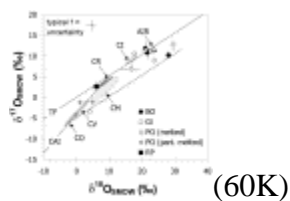


Fig. 14. Average oxygen isotopic compositions of individual type-S spherules calculated relative to standard mean ocean water (SMOW). The range bars associated with each data point give the variations from the mean within individual spherules, and do not represent the typical uncertainty for individual analyses, which is shown on the upper left corner of the plot. Data for spherule 94-4B-43 are given in [Figure 13](#) and are not reported here. The solid line labeled TF is the terrestrial fractionation line. The line labeled CAI was read from [Figure 2](#) of [Clayton \(1993\)](#); it has the form  $\delta^{17}\text{O} = 0.938 \times \delta^{18}\text{O} - 4.06$ . Data for CI, CM, CR, and CO chondrites represent whole-rock analyses of meteorite falls taken from [Rowe et al 1994](#), [Weisberg et al 1993](#) and [Bischoff et al 1993](#), and [Clayton and Mayeda 1984](#), [Clayton and Mayeda 1999](#) and [Clayton and Mayeda 2001](#).

Table 8.

Average oxygen isotope compositions of, and possible precursors for type-S spherules.

pdfMachine

Is a pdf writer that produces quality PDF files with ease!

Produce quality PDF files in seconds and preserve the integrity of your original documents. Compatible across nearly all Windows platforms, if you can print from a windows application you can use pdfMachine.

Get yours now!

Sample	Texture	$\delta^{18}\text{O}$ (‰) <sup>‡</sup>	$\delta^{17}\text{O}$ (‰) <sup>‡</sup>	$f_{\text{lost}}^{\pm}$	Affinity
94-4-11	BO	21.7 <sub>-1.9</sub> <sup>+2.2</sup>	10.7 <sub>-1.3</sub> <sup>+1</sup> .2	0.20 ‡	CI
94-4B-42	BO	28.1 <sub>-1.4</sub> <sup>+0.9</sup>	10.2 <sub>-0.5</sub> <sup>+0</sup> .8	0.70 ‡	CO/CV + fractionation or carbonate?
KK297-A-23	BO	21.1 <sub>-2.7</sub> <sup>+2.6</sup>	11.9 <sub>-1.1</sub> <sup>+1</sup> .7	0.18 ‡	CI
94-4B-25	GI	4.1 <sub>-0.7</sub> <sup>+0.8</sup>	-3.4 <sub>-0.0</sub> <sup>+0</sup> .0	0.16 ‡	CO + slight fractionation?
94-4-32	RP	6.2 <sub>-2.5</sub> <sup>+1.2</sup>	2.5 <sub>-0.8</sub> <sup>+1.3</sup>		CM/CR
94-4-14	PO	21.1 <sub>-1.1</sub> <sup>+1.1</sup>	11.4 <sub>-0.5</sub> <sup>+0</sup> .7	0.19 ‡	CI
94-4B-45	PO	23.7 <sub>-0.3</sub> <sup>+0.5</sup>	9.0 <sub>-0.0</sub> <sup>+0.0</sup>	0.64 ‡	CM/CV + fractionation or carbonate?
94-4B-26	PO	16.7 <sub>-3.2</sub> <sup>+2.7</sup>	6.9 <sub>-0.8</sub> <sup>+1.2</sup>	0.51 ‡	CM/CR + mixing/fractionation?
94-4-13	PO	29.5 <sub>-0.4</sub> <sup>+0.3</sup>	12.8 <sub>-1.6</sub> <sup>+0</sup> .9	0.71 ‡	CM/CV + fractionation or carbonate?
94-4-8	PO	17.7 <sub>-0.9</sub> <sup>+0.8</sup>	10.6 <sub>-0.0</sub> <sup>+0</sup> .0	0.06 ‡	CI
94-4-14B	PO <sup>‡</sup>	5.0 <sub>-4.3</sub> <sup>+3.9</sup>	-1.1 <sub>-1.8</sub> <sup>+1</sup> .7		CM/CV
94-4B-6	PO <sup>‡</sup>	-0.1	-4.2		CV
94-4B-12	PO <sup>‡</sup>	1.1	-1.1		CO/CV
94-4B-43	PO <sup>‡</sup>	11.9 <sub>-10.3</sub> <sup>+12</sup> .8	3.6 <sub>-8.6</sub> <sup>+6.4</sup>		?

<sup>‡</sup> Weighted mean value and range (when more than one analysis was made) for each particle. The precision of individual analyses is on the order of  $\sim 1$  ‰, see [Table 7](#).

<sup>±</sup> Lost fraction calculated according to [Wang et al. \(2001\)](#) with average CI ( $\delta^{18}\text{O} = 16.3$ ‰)

<sup>‡</sup> or CO/CM ( $\delta^{18}\text{O} = 0$ ‰)

<sup>‡</sup> starting compositions before evaporation.

pdfMachine

Is a pdf writer that produces quality PDF files with ease!

Produce quality PDF files in seconds and preserve the integrity of your original documents. Compatible across nearly all Windows platforms, if you can print from a windows application you can use pdfMachine.

Get yours now!

If we take as the starting material for each spherule the type of conventional carbonaceous chondrite that lies closest to it in the oxygen three-isotope plot ([Fig. 12](#)), then we do not need to calculate *large* evaporative losses of oxygen for most of the samples. The data for two of the BO and two of the melted PO spherules cited in (1) that plot close to the TF line can be explained by starting with CI-like material and either exchanging it with a phase high in  $\delta^{18}\text{O}$  and  $\delta^{17}\text{O}$  (atmospheric oxygen) or subjecting it to a small degree of mass-fractionation during melting and evaporation. This starting composition would be representative of bulk CI-like material, and not CI anhydrous minerals, which are rare and which have oxygen isotopic compositions close to the CAI mixing line ([Leshin et al., 1997](#)). The radial pyroxene, as well as the PO partially melted spherules that plot near the field of carbonaceous chondrites, likely contain dominantly indigenous extraterrestrial oxygen, which was essentially unfractionated during atmospheric entry heating. The glass spherule could also be explained by a CO-like precursor that underwent minimal mass fractionation. The only really puzzling samples that are difficult to explain in this scenario are the BO and the three PO spherules in group (1) that plot below the TF line (94-4B-26, 94-4B-42, 94-4B-45 and 94-4-13). These spherules plot close to fractionation lines starting from CM- or CO-like compositions, but this would require large evaporative losses (see [Section 6.5](#)). They also plot close to mixing lines between CM- or CO-like compositions and the field of carbonates analyzed in CM chondrites ([Brearley et al 1999](#) and [Benedix et al 2003](#)) and in Orgueil and Tagish Lake ([Engrand et al 2001a](#), [Engrand et al 2001b](#) and [Leshin et al 2001](#)). As we cannot rule out the possibility of significant mass-dependent fractionation for these spherules, it would be helpful to know the isotopic compositions of the other elements they contain.

### 6.3. Relation between Oxygen Isotope Data and Spherule Texture

[Taylor et al. \(2000\)](#) have proposed a textural classification sequence for the type-S spherules that corresponds to increasing degrees of heating: relict-grain-bearing < porphyritic < barred olivine < cryptocrystalline < glass < Ca-Al-Ti rich or CAT. Our samples include one or more spherules of the porphyritic, barred olivine, and glass types. In agreement with this sequence, the data show that for the partially melted spherules porphyritic olivine, the average  $\delta^{18}\text{O} = (4 \pm 5)\text{‰}$  and  $\delta^{17}\text{O} = (-1 \pm 3)\text{‰}$  values are lower than the values found for the totally melted porphyritic olivine spherules (averages  $\delta^{18}\text{O} = (22 \pm 5)\text{‰}$  and  $\delta^{17}\text{O} = (10 \pm 2)\text{‰}$ ) which are in turn slightly lower than the mean isotopic values measured for barred-olivine spherules ( $\delta^{18}\text{O} = (24 \pm 4)\text{‰}$  and  $\delta^{17}\text{O} = (11 \pm 1)\text{‰}$ ). On the other hand, to follow this sequence, we expect the glass particle 94-4B-25 to have high values of  $\delta^{18}\text{O}$  and  $\delta^{17}\text{O}$  contrary to observation ([Table 7](#), [Fig. 14](#)). Relative to the BO spherules, however, this particle is more enriched in refractory elements such as Al and Ca, and contains less Fe, as expected from a higher temperature event. To explain the unexpectedly low isotopic fractionation of oxygen of this spherule, one can invoke very low values for  $\delta^{18}\text{O}$  and  $\delta^{17}\text{O}$  of the starting material, a loss by ablation and not evaporation during heating, or a starting composition with unusually high concentrations of Al and Ca. This spherule could also constitute a chondrule fragment that survived the atmospheric entry mostly unmelted. The preexisting refractory chemical composition of this spherule would have protected the spherule from a large amount of evaporation. Our samples also include two particles with textures whose positions in the proposed heating sequence are unspecified, the radial pyroxene spherule 94-4-32 ([Fig. 11b](#)) and the

pdfMachine

Is a pdf writer that produces quality PDF files with ease!

Produce quality PDF files in seconds and preserve the integrity of your original documents. Compatible across nearly all Windows platforms, if you can print from a windows application you can use pdfMachine.

Get yours now!

porphyritic particle 94-4-14B (Fig. 11e). Among FeO-rich chondrules, radial-pyroxene chondrules tend to be less refractory than porphyritic types (Wasson, 1996), which is at least qualitatively consistent with our spherule observations, since the observed  $\delta^{18}\text{O}$  and  $\delta^{17}\text{O}$  values for the RP spherule average ( $6.2 \pm 1.7$ )‰, and ( $2.8 \pm 1.1$ )‰, respectively. The data for this particle actually plot in the field of unmelted minerals in Antarctic micrometeorites (Engrand et al., 1999) and we consider that this grain may constitute a remnant of a chondrule fragment that reached the Earth's surface unmelted. Interestingly, igneous material rims the top and bottom of spherule 94-4-32 (shown by arrows on Fig. 11b) that could have formed by atmospheric melting of matrix material that originally surrounded the chondrule (Genge, 2004). In addition to the candidate 94-4B-25 discussed above, this would be one of the few well preserved chondrules found in the Antarctic micrometeorite collections (e.g., Engrand and Maurette 1998 and Genge et al 2005). One data point from the core of the porphyritic particle 94-4-14B plots very close to the CM whole-rock field on the oxygen three isotope diagram. The other data point taken in the melted rim of the particle 94-4-14B shows some isotopic fractionation. This grain could have remained largely unmelted during atmospheric entry, at least in the interior of the grain, and thereby kept most of its extraterrestrial oxygen.

#### 6.4. Additional Evidence for Small Evaporative Losses of Oxygen from Type S Spherules

As a first evidence of small losses by evaporation in type-S spherules, we note that no correlation between the apparent size of the spherules and the degree of isotopic fractionation is found. One might expect such a correlation if evaporation were extensive, especially because a correlation *is* observed for our type C iron oxide spherules, which did undergo large degrees of evaporation (Fig. 3b).

Based on a consideration of the isotopic fractionations of elements other than oxygen, we also believe that the fractionation of oxygen isotopes by evaporation is small for most of our samples.

The iron isotopes in the two type-S spherules analyzed here are only weakly fractionated (Table 3). In a study of over 40 stony cosmic spherules, Taylor et al. (2002) found only 9 that showed significant fractionation of iron ( $\Phi_{\text{Fe}} > 5\text{‰/amu}$ ). However, iron depletion observed in cosmic spherules is rather explained from the separation (and loss) of immiscible phases than from evaporation of significant amounts of iron (e.g. Brownlee 1985, Genge and Grady 1998 and Alexander et al 2002). The low degrees of iron isotopic fractionation observed are therefore a weak basis on which to draw conclusions about oxygen, which is not involved in the main process of iron loss.

While the Cr isotopes are appreciably fractionated, the Cr abundance is too low (as noted above) to have had much effect on oxygen isotope abundances, and, indeed, fractionation of Cr may involve sulfur rather than oxygen. Chromium only exhibits a chalcophile tendency at low oxygen fugacity. A likely cause of reduction would be the pyrolysis of carbonaceous material present in the incoming stony micrometeoroids, thus linking them to fine-grained micrometeorites.

If so, oxygen must evaporate in some form, however, and the next most volatile element that is a major partner for oxygen is silicon. Alexander et al. (2002) report the Mg, Si and Fe isotopic compositions in five stony CAT spherules which are very enriched in refractory elements and are thought to have been much more strongly heated than typical barred olivine spherules. For a given cosmic spherule they typically find relatively low

pdfMachine

Is a pdf writer that produces quality PDF files with ease!

Produce quality PDF files in seconds and preserve the integrity of your original documents. Compatible across nearly all Windows platforms, if you can print from a windows application you can use pdfMachine.

Get yours now!

degrees of isotopic fractionations  $\Phi_{\text{Mg}}(\sim 0\text{‰/amu}) < \Phi_{\text{Si}}(\sim 2\text{‰/amu}) < \Phi_{\text{Fe}}(\sim 5\text{‰/amu})$ . In only one of these particles did the loss of Si reach more than 50%, with a Mg loss of  $\sim 40\%$  and a loss of iron of  $\sim 100\%$  (most of the iron is lost as immiscible phases formed during melting, see above). These CAT spherules being probably the most heated class of cosmic spherules, [Alexander et al. \(2002\)](#) state that the other stony micrometeorites and cosmic spherules will not have lost significant masses of Al, Mg, Si, or Ca by evaporation. Other attempts to detect isotopic fractionation of Mg isotopes in spherules (e.g., [Davis et al 1991](#), [Misawa et al 1992](#), [Schnabel et al 1999](#) and [Yada et al 2003a](#)) have yielded only a few positive results. These generally negative findings suggest that either the oxygen in the type-S spherules undergoes little mass-dependent fractionation (the inference we favor), or that if it does fractionate, the fractionation occurs on a path not associated with Fe, Si, or Mg.

### 6.5. Evaporative Loss from Barred Olivine Spherules

For completeness, we calculate from the Rayleigh equation the likely degree of evaporative loss of oxygen from the barred olivine (BO) and the totally melted porphyritic olivine (PO) spherules of [Figure 14 \(Table 8\)](#). We assume homogeneous melts and the fractionation factor determined by [Wang et al. \(2001\)](#) and divide the objects into two subgroups. One subgroup comprises the BO and PO spherules (94-4-11, KK2-97A-23, 94-4-14 and 94-4-8) with values of  $\delta^{18}\text{O}$  and  $\delta^{17}\text{O}$  that can be reached by mass-dependent fractionation of oxygen with the isotopic composition found in CI chondrites ([Fig. 14, Table 8](#)). The calculated fractional losses for this group are relatively small, ranging from 0.1 (10%) to 0.2 (20%). The other subgroup, the spherules 94-4B-42, 94-4B-45, 94-4B-26, and 94-4-13, comprises the spherules with high values of  $\delta^{18}\text{O}$  and  $\delta^{17}\text{O}$ , but which fall below the TF line ([Fig. 14, Table 8](#)). They are more consistent with mass-dependent fractionation of oxygen with the isotopic composition found in CO/CV and CM/CR meteorites. The calculated fractional losses for this group are larger, in the range from 0.5 to 0.7. We consider these fractions to be upper bounds.

### 6.6. Isotopically Heterogeneous Spherule 94-4B-43

The oxygen isotope abundances in porphyritic spherule 94-4B-43 vary significantly, with  $\delta^{18}\text{O}$  ranging between 1.5‰ to 24.7‰. The data from this spherule are plotted in [Figure 13](#) keyed to their locations in the particle. To interpret such a large range of isotopic values by a mass fractionation process (e.g., Rayleigh distillation) would imply total melting and homogenization of the particle, followed by the evaporation of a large fraction of the oxygen. This hypothesis is inconsistent with the texture and chemical composition of the spherule, which show that the particle did not equilibrate. The matrix of the spherule has an oxygen isotopic composition very close to that of air, which alternatively suggests isotopic mixing/exchange with atmospheric oxygen. The observed  $\delta^{18}\text{O}$  values of 14.5‰ and 16.8‰ ([Fig. 13](#)) may be explained by physical mixing in the beam spot of relict forsterite grains (bearing extraterrestrial oxygen) and fractionated matrix. However, one forsteritic olivine grain ( $\text{Fo}_{98.7}$ ) within this spherule has an oxygen isotopic composition ( $\delta^{18}\text{O} = 1.5\text{‰}$ ) close to the field of the unmelted micrometeorites ([Engrand et al., 1999](#)) while a second olivine grain at the border of the CS which has nearly identical elemental composition ( $\text{Fo}_{98.8}$ ) is  $\sim 10\text{‰}$  heavier in  $\delta^{18}\text{O}$  (13.4‰). To reproduce the measured oxygen isotopic compositions of the  $\text{Fo}_{98.8}$  grain ( $\delta^{18}\text{O} \sim 13.4\text{‰}$ ), one would need  $\sim 60\%$  isotopic exchange between indigenous oxygen (postulated at  $\delta^{18}\text{O} \sim 0\text{‰}$ ) and atmospheric oxygen ( $\delta^{18}\text{O} \sim 23.5\text{‰}$ ) and/or oxygen coming from matrix

which equilibrated with air. [Gérard and Jaoul \(1989\)](#) have measured the oxygen diffusion rates for San Carlos olivine ( $F_{O90}$ ). In our case ( $F_{O98.5}$ ), the oxygen diffusion coefficient has to be scaled from that of [Gérard and Jaoul \(1989\)](#) as the diffusion coefficient is proportional to the concentration of iron in the olivine to the power of one third (see Eqn. 4 in [Gérard and Jaoul \(1989\)](#)). For a 10  $\mu\text{m}$   $F_{O98.5}$  grain, the 60% isotopic exchange could be achieved within 40 s at 1800°C. These conditions are marginally compatible with those of atmospheric entry heating for cosmic spherules (e.g., [Toppani et al., 2001](#)). Although one might expect the spherule to be completely melted at this temperature and duration of heating, [Greenwood and Hess \(1995\)](#) suggest that in the case of flash heating refractory minerals like forsterite could melt in situ, within a preexisting melt of less refractory minerals (iron-rich matrix in this case) without complete mixing of the two components. In this case, the olivine grains are not truly “relict.” Considering the temperature and duration of heating quoted above,  $\sim 35\%$  of the Fe and Mg should have exchanged between the forsteritic olivines and the Fe-rich matrix, according to experiments by [Chakraborty \(1997\)](#). This result is compatible with the observation of Fe-rich zoning around the forsterite grains in this spherule ([Fig. 13](#)). Thus, the somewhat puzzling oxygen isotopic composition of this peculiar spherule can be interpreted as a result of oxygen self-diffusion between the incident micrometeoroid and atmospheric oxygen at high temperature.

## 7. Conclusions

We have measured the O, Cr, Fe, Ni isotopes in eleven type-I (iron) deep-sea spherules, the oxygen isotopic composition of 13 type-S (stony) Antarctic and one stony deep-sea spherule, and the Fe and Cr isotopic composition of two other type-S deep-sea spherules. Type-I spherules show large enrichments of the heavier isotopes of O, Cr, Fe, Ni, by anywhere from a few ‰/amu to 50 ‰/amu. The isotopic fractionation and isotopic homogeneity of the type-I spherules are consistent with a Rayleigh distillation of the molten objects as they evaporate during their passage through the Earth’s atmosphere. As heating and oxidation progress, the spherules lose their metallic cores. Later-stage melts are richer in oxygen and freeze to form solids with larger fractions of magnetite and magnetite rims. Larger degrees of isotopic fractionation generally correlate with texture and degree of oxidation.

Previous analyses of pooled type-I samples have established that oxygen isotopes fractionate in type-I spherules ([Clayton et al., 1986](#)), but not on average by so much as do the metals (e.g., [Herzog et al., 1999](#)). Our new results show directly that the isotopic fractionation of oxygen in individual spherules increases systematically with but lags behind that of the metals measured in the same spherules. We conclude that: 1) some metal evaporates and fractionates before oxygen can react with it and that as a result, the fractionation of metal jumps to an early lead that oxygen cannot overtake; and 2) during the later stages of spherule evolution, iron and chromium oxidize completely and thereafter evaporate as oxides, thereby fractionating the oxygen. A portion of the fractionation of oxygen, however may occur through a different mechanism, namely, a kinetic isotope effect associated with the chemical combination of atmospheric oxygen with the molten object. Assuming that the kinetic isotope effect lowers the  $\delta^{18}\text{O}$  value by up to 8‰ (e.g., [Clayton et al., 1986](#)), we estimate that the oxidation of iron and chromium in the average type-I spherule was complete by the time that 10 to 40% of the iron had evaporated. Most of the evaporation of oxygen appears to be tied to that of Fe by virtue

pdfMachine

Is a pdf writer that produces quality PDF files with ease!

Produce quality PDF files in seconds and preserve the integrity of your original documents. Compatible across nearly all Windows platforms, if you can print from a windows application you can use pdfMachine.

Get yours now!

of iron's large abundance and because nickel, the next most abundant metal, resists oxidation longer.

The scarcity of type-I spherules with small degrees of mass-dependent isotopic fractionation in Fe, Cr, and Ni isotopic ratios suggests that once the metallic melts have formed, their evaporation occurs very rapidly.

The oxygen isotope abundances of stony (type-S) cosmic spherules vary a great deal, by nearly 30‰ for  $\delta^{18}\text{O}$ , but not solely as a result of mass-dependent fractionation. Several circumstantial lines of evidence point to relatively small evaporative effects in many though not all type-S spherules. Those lines of evidence include good matches of the oxygen isotope data to known types of carbonaceous chondrites and the absence of common and large isotopic effects in other elements that ought to evaporate with oxygen (see [Alexander et al 2002](#) and [Taylor et al 2002](#)). However, despite the generally small degrees of isotopic fractionation so far observed for Fe, Si, and Mg in type-S spherules, it appears that some minor and trace elements may record evaporative losses and/or oxygen may exchange with air during melting. In the two type-S spherules analyzed isotopically for Cr, evaporative losses calculated from the Rayleigh equation exceed 50%.

Although total mass losses due to evaporation were probably small for most type-S spherules, typically <20% for major elements, heating was sufficiently pronounced and varied to have created a fairly well documented sequence of textural types ([Taylor et al., 2000](#)). Consistent with the proposed heating/textural sequence, porphyritic-partially melted spherules tend to have lower values of  $\delta^{18}\text{O}$ . In contrast to this sequence, a glass cosmic spherule has only slightly fractionated oxygen isotopic composition. It could be a largely unmelted chondrule fragment. Another of the type-S spherules studied, 94-4-32, has no assigned place in the textural hierarchy of heating. On the one hand, it looks similar to several strongly heated objects, while on the other its oxygen isotope composition is unfractionated and similar to those of many chondrules. We infer that this object is a fragment of a chondrule that survived unmelted upon atmospheric entry. The significance of this observation lies not only in the conclusion that the type-S spherules include chondrules, but also in the implication that improved understanding of how type-S spherules formed will allow us to distinguish more unusual and interesting objects.

Type-I spherules show generally larger degrees of isotopic fractionation than type-S spherules. Possible explanations include: a) the short duration of the heating pulse associated with the high volatile content of the type-S spherule precursors compared to type-I spherules; b) higher evaporation temperatures for at least a refractory portion of the silicates compared to that of iron metal or oxide; c) lower duration of heating of type-S spherules compared to type-I spherules as a consequence of their lower densities.

The isotopic results on these spherules, formed by transient heating at the top of the atmosphere, are interesting in their own right but they may also provide insight into other areas of study such as the origin of chondrules and perhaps even processes on Mars.

Chondrules also form by transient heating but they do not show the levels of isotopic fractionation seen in the cosmic spherules. That they do not, provides clues to the nature of the relatively constrained conditions that produced chondrules. Cosmic spherules, accumulated over billions of years, must be highly abundant in some of the martian soils. This may be particularly true in cases where lag deposits form by winnowing processes.

The isotopic character of the spherules could provide clues to past martian processes and environments. The presence of a significant abundance of spherules in a soil sample

**pdfMachine**

**Is a pdf writer that produces quality PDF files with ease!**

Produce quality PDF files in seconds and preserve the integrity of your original documents. Compatible across nearly all Windows platforms, if you can print from a windows application you can use pdfMachine.

Get yours now!

might also cause small but confusing effects in its bulk isotopic composition.

---

### Acknowledgments

We thank G. Lofgren for his critical comments, which helped improve the manuscript. Insightful discussions with O. Jaoul, A. Toppani, and G. J. Greenwood are acknowledged. The paper was improved by thoughtful reviews of S. Taylor and M. J. Genge. This work was supported by grants from the NASA Cosmochemistry program (NAG5-11719 to GFH, NAG5-11809 to LAL). The UCLA ion microprobe facility is partially supported by a grant from the NSF Instrumentation and Facilities Program.  
*Associate editor:* C. Koeberl

---

### References

- [Alexander et al 2002](#) C.M.O.D. Alexander, S. Taylor, J. Delaney, P. Ma and G.F. Herzog, Mass dependent fractionation of Mg, Si and Fe isotopes in five stony micrometeorites, *Geochim. Cosmochim. Acta* **66** (2002), pp. 173–183. [SummaryPlus](#) | [Full Text + Links](#) | [PDF \(372 K\)](#)
- [Anders and Grevesse 1989](#) E. Anders and N. Grevesse, Abundances of the elements Meteoritic and solar, *Geochim. Cosmochim. Acta* **53** (1989), pp. 197–214. [Abstract](#) | [Abstract + References](#) | [PDF \(2689 K\)](#)
- [Benedix et al 2003](#) G.K. Benedix, L.A. Leshin, J. Farquhar, T.L. Jackson and M.H. Thiemens, Carbonates in CM2 chondrites Constraints on alteration conditions from oxygen isotopic compositions and petrographic observations, *Geochim. Cosmochim. Acta* **67** (2003), pp. 1577–1588. [Abstract](#) | [Abstract + References](#) | [PDF \(575 K\)](#)
- [Birck and Allegre 1985](#) J.-L. Birck and C.-J. Allegre, Evidence for the presence of  $^{53}\text{Mn}$  in the early solar system, *Geophys. Res. Lett* **12** (1985), pp. 745–748. [Abstract-INSPEC](#)
- [Bischoff et al 1993](#) A. Bischoff, H. Palme, R.D. Ash, R.N. Clayton, L. Schultz, U. Herpers, D. Stoffler, M.M. Grady, C.T. Pillinger, B. Spettel, H. Weber, T. Grund, M. Endress and D. Weber, Paired Renazzo-type (CR) carbonaceous chondrites from the Sahara, *Geochim. Cosmochim. Acta* **57** (1993), pp. 1587–1603. [Abstract](#) | [Abstract + References](#) | [PDF \(2189 K\)](#)
- [Brearley et al 1999](#) A.J. Brearley, J.M. Saxton, I.C. Lyon and G. Turner, Carbonates in the Murchison CM chondrite CL characteristics and oxygen isotopic compositions (abstract), *Lunar Planet. Sci* **30** (1999), p. 1301.
- [Brownlee 1985](#) D.E. Brownlee, Cosmic dust Collection and research, *Ann. Rev. Earth Planet. Sci* **13** (1985), pp. 147–173.
- [Brownlee et al 1997](#) D.E. Brownlee, B. Bates and L. Schramm, The elemental composition of stony cosmic spherules, *Meteor. Planet. Sci* **32** (1997), pp. 157–175. [Abstract-GEOBASE](#) | [Abstract-INSPEC](#)
- [Chakraborty 1997](#) S. Chakraborty, Rates and mechanisms of Fe-Mg interdiffusion in olivine at 980°C–1300°C, *J. Geophys. Res* **102** (1997) (12), pp. 12,317–12,331.
- [Clayton and Mayeda 1984](#) R.N. Clayton and T.K. Mayeda, The oxygen isotope record in Murchison and other carbonaceous chondrites, *Earth Planet. Sci. Lett* **67** (1984), pp. 151–161. [Abstract](#) | [Abstract + References](#) | [PDF \(742 K\)](#)

pdfMachine

Is a pdf writer that produces quality PDF files with ease!

Produce quality PDF files in seconds and preserve the integrity of your original documents. Compatible across nearly all Windows platforms, if you can print from a windows application you can use pdfMachine.

Get yours now!

[Clayton et al 1986](#) R.N. Clayton, T.M. Mayeda and D.E. Brownlee, Oxygen isotopes in deep-sea spherules, *Earth Planet. Sci. Lett* **79** (1986), pp. 235–240. [SummaryPlus](#) | [Full Text + Links](#) | [PDF \(480 K\)](#)

[Clayton 1993](#) R.N. Clayton, Oxygen isotopes in meteorites, *Ann. Rev. Earth Planet. Sci* **21** (1993), pp. 115–149. [Abstract-GEOBASE](#)

[Clayton and Mayeda 1999](#) R.N. Clayton and T.K. Mayeda, Oxygen isotope studies of carbonaceous chondrites, *Geochim. Cosmochim. Acta* **63** (1999), pp. 2089–2104. [Abstract-GEOBASE](#) | [Abstract-INSPEC](#)

[Clayton and Mayeda 2001](#) R.N. Clayton and T.K. Mayeda, Oxygen isotopic composition of the Tagish Lake carbonaceous chondrite (abstract), *Lunar Planet. Sci* **32** (2001), p. 1885.

[Czajkowski 1987](#) J. Czajkowski, *Cosmo and geochemistry of the Jurassic hardgrounds*, Ph.D. diss. University of California, San Diego (1987).

[Davis et al 1991](#) A.M. Davis, R.N. Clayton, T.K. Mayeda and D.E. Brownlee, Large mass fractionation of iron isotopes in cosmic spherules collected from deep-sea sediments (abstract), *Lunar Planet. Sci* **22** (1991), pp. 281–282.

[Davis and Brownlee 1993](#) A.M. Davis and D.E. Brownlee, Iron and nickel isotopic mass fractionation in deep-sea spherules (abstract), *Lunar Planet. Sci* **24** (1993), pp. 373–374.

[Delaney et al 2002](#) J. Delaney, G.F. Herzog, P. Ma, C.M.O.D. Alexander and S. Taylor, The fate of metal ejected from stony cosmic spherules Low chrome on the range (abstract), *Meteor. Planet. Sci* **37** (2002) (Suppl.), p. A41.

[Duprat et al 2005](#) J. Duprat, C. Engrand, M. Maurette, M. Gounelle, G. Kurat and H. Leroux, Friable micrometeorites from central Antarctica snow (abstract), *Lunar Planet. Sci* **36** (2005), p. 1678.

[Engrand and Maurette 1998](#) C. Engrand and M. Maurette, Carbonaceous micrometeorites from Antarctica, *Meteor. Planet. Sci* **33** (1998), pp. 565–580. [Abstract-MEDLINE](#) | [Abstract-INSPEC](#)

[Engrand et al 1999](#) C. Engrand, K.D. McKeegan and L.A. Leshin, Oxygen isotopic compositions of individual minerals in Antarctic micrometeorites Further links to carbonaceous chondrites, *Geochim. Cosmochim. Acta* **63** (1999), pp. 2623–2636. [SummaryPlus](#) | [Full Text + Links](#) | [PDF \(607 K\)](#)

[Engrand et al 2001a](#) C. Engrand, M. Gounelle, J. Duprat and M.E. Zolensky, In-situ oxygen isotopic composition of individual minerals in Tagish Lake, a new type 2 carbonaceous meteorite (abstract), *Lunar Planet. Sci* **32** (2001), p. 1568.

[Engrand et al 2001b](#) C. Engrand, M. Gounelle and M.E. Zolensky, Oxygen isotopic composition of Tagish Lake (abstract), *Meteor. Planet. Sci* **36** (2001) (Suppl.), p. A54.

[Fahey 1988](#) A.J. Fahey, *Ion microprobe measurement of Mg, Ca, Ti and Fe isotopic ratios and trace element abundances in hibonite-bearing inclusions from primitive meteorites*. Ph.D. diss., Washington University (1988).

[Genge 2004](#) M.J. Genge, Igneous rims on micrometeorites and the sizes of chondrules in main belt asteroids (abstract), *Lunar Planet. Sci* **35** (2004), p. 1102.

[Genge and Grady 1998](#) M.J. Genge and M.M. Grady, Melted micrometeorites from Antarctic ice with evidence for the separation of immiscible Fe-Ni-S liquids during entry heating, *Meteor. Planet. Sci* **33** (1998), pp. 425–434. [Abstract-GEOBASE](#) | [Abstract-INSPEC](#)

pdfMachine

Is a pdf writer that produces quality PDF files with ease!

Produce quality PDF files in seconds and preserve the integrity of your original documents. Compatible across nearly all Windows platforms, if you can print from a windows application you can use pdfMachine.

Get yours now!

[Genge et al 2005](#) M.J. Genge, A. Gileski and M.M. Grady, Chondrules in Antarctic micrometeorites, *Meteor. Planet. Sci* **40** (2005), pp. 225–238. [Abstract-INSPEC](#) | [Abstract-GEOBASE](#)

[Gerard and Jaoul 1989](#) O. Gérard and O. Jaoul, Oxygen diffusion in San Carlos olivine, *J. Geophys. Res* **94** (1989), pp. 4119–4128. [Abstract-GEOBASE](#)

[Gonfiantini et al 1993](#) Gonfiantini R., Stichler W., and Rozanski K. (1993) Standards and intercomparison materials distributed by the International Atomic Energy Agency for stable isotopes measurements. In *Reference and Intercomparison Materials for Stable Isotopes of Light Elements*, Vol. IAEA-Tecdoc-825, pp. 13–29. International Atomic Energy Agency.

[Greenwood and Hess 1995](#) J.P. Greenwood and P.C. Hess, Dissolution and melting kinetics Applications to chondrules (abstract), *Lunar Planet. Sci* **26** (1995), pp. 505–506.

[Herzog et al 1999](#) G.F. Herzog, S. Xue, G.S. Hall, L.E. Nyquist, C.Y. Shih, H. Wiesmann and D.E. Brownlee, Isotopic and elemental composition of iron, nickel and chromium in type-I deep-sea spherules Implications for origin and composition of the parent micrometeoroids, *Geochim. Cosmochim. Acta* **63** (1999), pp. 1443–1457. [SummaryPlus](#) | [Full Text + Links](#) | [PDF \(336 K\)](#)

[Kurat et al 1994](#) G. Kurat, C. Koeberl, T. Presper, F. Brandstätter and M. Maurette, Petrology and geochemistry of Antarctic micrometeorites, *Geochim. Cosmochim. Acta* **58** (1994), pp. 3879–3904. [Abstract](#) | [Abstract + References](#) | [PDF \(3047 K\)](#)

[Lal and Jull 2002](#) D. Lal and A.J.T. Jull, Atmospheric cosmic dust fluxes in the size range  $10^{-4}$  to 10 centimeters, *Astrophys. J* **576** (2002), pp. 1090–1097. [Full Text via CrossRef](#)

[Leshin et al 1997](#) L.A. Leshin, A.E. Rubin and K.D. McKeegan, The oxygen isotopic composition of olivine and pyroxene from CI chondrites, *Geochim. Cosmochim. Acta* **61** (1997), pp. 835–845. [SummaryPlus](#) | [Full Text + Links](#) | [PDF \(1542 K\)](#)

[Leshin et al 2001](#) L.A. Leshin, J. Farquhar, Y. Guan, S. Pizzarello, T.L. Jackson and M.H. Thiemens, Oxygen isotopic anatomy of Tagish Lake Relationship to primary and secondary minerals in CI and CM chondrites (abstract), *Lunar Planet. Sci* **32** (2001), p. 1843.

[Love and Brownlee 1993](#) S.G. Love and D.E. Brownlee, A direct measurement of the terrestrial mass accretion rate of cosmic dust, *Science* **262** (1993), pp. 550–553. [Abstract-INSPEC](#) | [Abstract-GEOBASE](#)

[Maurette et al 1994](#) M. Maurette, G. Immel, C. Hammer, R. Harvey, G. Kurat and S. Taylor, Collection and curation of IDPs from the Greenland and Antarctic ice sheets. In: M.E. Zolensky, T.L. Wilson, F.J.M. Rietmeijer and G.J. Flynn, Editors, *Analysis of Interplanetary Dust, AIP Conference Proceedings* (Vol. 310), American Institute of Physics (1994), pp. 277–289.

[Misawa et al 1992](#) K. Misawa, K. Yamakoshi and N. Nakamura, Mg isotopic compositions of stony spherules from deep-sea sediments, *Geochem. J* **26** (1992), pp. 29–36. [Abstract-OceanBase](#) | [Abstract-GEOBASE](#)

[Nyquist et al 1994](#) L.E. Nyquist, B. Bansal, H. Wiesmann and C.-Y. Shih, Neodymium, strontium and chromium isotopic studies of the LEW86010 and Angra dos Reis meteorites and the chronology of the angrite parent body, *Meteoritics* **28** (1994), pp. 872–885. [Abstract-INSPEC](#) | [Abstract-GEOBASE](#)

pdfMachine

Is a pdf writer that produces quality PDF files with ease!

Produce quality PDF files in seconds and preserve the integrity of your original documents. Compatible across nearly all Windows platforms, if you can print from a windows application you can use pdfMachine.

Get yours now!

[Raisbeck et al 1982](#) G.M. Raisbeck, F. Yiou, J. Klein, R. Middleton and Y. Yamakoshi, Measurement of  $^{26}\text{Al}$  and  $^{10}\text{Be}$  in extraterrestrial matter by accelerator mass spectrometry, *Meteoritics* **17** (1982), pp. 270–271.

[Rowe et al 1994](#) M.W. Rowe, R.N. Clayton and T.K. Mayeda, Oxygen isotopes in separated components of CI and CM meteorites, *Geochim. Cosmochim. Acta* **58** (1994), pp. 5341–5347. [Abstract](#) | [Abstract + References](#) | [PDF \(828 K\)](#)

[Schnabel et al 1999](#) C. Schnabel, G.F. Herzog, S. Taylor, P. Field and R. Sherrell, Magnesium isotope abundances in stony Antarctic micrometeorites, *Antarc. Meteorite Res* **24** (1999), pp. 166–167.

[Taylor et al 2000](#) S. Taylor, J.H. Lever and R.P. Harvey, Numbers, types and compositions of an unbiased collection of cosmic spherules, *Meteor. Planet. Sci* **35** (2000), pp. 651–666. [Abstract-GEOBASE](#) | [Abstract-INSPEC](#)

[Taylor et al 2002](#) S. Taylor, C.M.O.D. Alexander, J. Delaney, P. Ma, G.F. Herzog and C. Engrand, Isotopic fractionation of Fe-57 in stony cosmic spherules Implications for iron loss (abstract), *Lunar Planet. Sci* **33** (2002), p. 1136.

[Thiemens et al 1995](#) M. Thiemens, T. Jackson, E.C. Zipf, P.W. Erdman and C. Van Egmond, Carbon dioxide and oxygen isotope anomalies in the mesosphere and stratosphere, *Science* **270** (1995), pp. 969–972. [Abstract-GEOBASE](#)

[Toppani et al 2001](#) A. Toppani, G. Libourel, C. Engrand and M. Maurette, Experimental simulation of atmospheric entry of micrometeorites, *Meteor. Planet. Sci* **36** (2001), pp. 1377–1396. [Abstract-GEOBASE](#)

[Völkening and Papanastassiou 1989](#) J. Völkening and D.A. Papanastassiou, Iron isotope anomalies, *Astrophys. J* **347** (1989), pp. L43–L46.

[Wang et al 1994](#) J. Wang, A.M. Davis, R.N. Clayton and T.K. Mayeda, Kinetic isotopic fractionation during the evaporation of the iron oxide from liquid state (abstract), *Lunar Planet. Sci* **25** (1994), pp. 1459–1560.

[Wang et al 2001](#) J. Wang, A.M. Davis, R.N. Clayton, T.K. Mayeda and A. Hashimoto, Chemical and isotopic fractionation during the evaporation of the FeO-MgO-SiO<sub>2</sub>-CaO-Al<sub>2</sub>O<sub>3</sub>-TiO<sub>2</sub> rare earth element melt system, *Geochim. Cosmochim. Acta* **65** (2001), pp. 479–494. [SummaryPlus](#) | [Full Text + Links](#) | [PDF \(831 K\)](#)

[Wasson 1996](#) J.T. Wasson, Chondrule formation Energetics and length scales. In: R.H. Hewins, R.H. Jones and E.R.D. Scott, Editors, *Chondrules and the Protoplanetary Disk*, Cambridge University Press (1996), pp. 45–54.

[Weisberg et al 1993](#) M.K. Weisberg, M. Prinz, R.N. Clayton and T.K. Mayeda, The CR (Renazzo-type) carbonaceous chondrite group and its implications, *Geochim. Cosmochim. Acta* **57** (1993), pp. 1567–1586. [Abstract](#) | [Abstract + References](#) | [PDF \(2577 K\)](#)

[Williamson 1968](#) J.H. Williamson, Least-squares fitting of straight line, *Can. J. Phys* **46** (1968), pp. 1845–1847.

[Xue et al 1995](#) S. Xue, G.F. Herzog, G.S. Hall, D. Bi and D.E. Brownlee, Nickel isotope abundances of type-I deep-sea spheres and of iron-nickel spherules from sediments in Alberta, Canada, *Geochim. Cosmochim. Acta* **59** (1995), pp. 4975–4981. [SummaryPlus](#) | [Full Text + Links](#) | [PDF \(923 K\)](#)

[Yada et al 1996](#) T. Yada, T. Nakamura, M. Sekiya and N. Takaoka, Formation processes of magnetic spherules collected from deep-sea sediments—Observations and numerical

simulations of the orbital evolution, *Proc. NIPR Symp. Antarc. Meteorites* **9** (1996), pp. 218–236.

[Yada et al 2002](#) T. Yada, N. Matsumoto, T. Nakamura, T. Noguchi, T. Setoyanagi, N. Takaoka and H. Kojima, Oxygen isotopic composition mineral grains in Antarctic micrometeorites and bulk spherules A spherule having large  $\Delta^{17}\text{O}$  (abstract), *Meteor. Planet. Sci* **37** (2002) (Suppl), p. A152.

[Yada et al 2003a](#) T. Yada, T. Nakamura, T. Noguchi, T. Ushikubo, H. Hiyagon and N. Sugiura, Mg, Si and Fe fractionation observed in Antarctic silicate spherules, *Meteor. Planet. Sci* **38** (2003) (Suppl), p. A88.

[Yada et al 2003b](#) T. Yada, T. Nakamura, T. Noguchi, T. Ushikubo, N. Matsumoto, H. Kojima and N. Takaoka, Variations of oxygen isotopic compositions of silicate spherules collected from Antarctic blue ice (abstract), *Lunar Planet. Sci* **34** (2003), p. 1587.

[Yada et al 2003c](#) T. Yada, T. Nakamura, T. Noguchi, T. Ushikubo, N. Matsumoto, H. Kojima and N. Takaoka, Estimation for precursors of silicate spherules based on their oxygen isotopic compositions (abstract), *International Symposium on Evolution of Solar System Materials A New Perspective from Antarctic Meteorites*, National Institute of Polar Research, Tokyo, Japan (2003), pp. 146–147.

[Yiou et al 1985](#) F. Yiou, G.M. Raisbeck and D.E. Brownlee,  $^{10}\text{Be}$  in iron type cosmic spherules Evidence for a differentiated parent body (abstract), *Meteoritics* **20** (1985), p. 791.



Author to whom correspondence should be addressed, at CSNSM Bat. 104, 91405 Orsay Campus, France

† *Present address:* Department of Geological Sciences and Center for Meteorite Studies, Arizona State University, Tempe, AZ 85287-1404, USA.

‡ *Present address:* Scottish Universities Environmental Research Centre, Rankine Avenue, East Kilbride G75 0QF, Scotland.

pdfMachine

Is a pdf writer that produces quality PDF files with ease!

Produce quality PDF files in seconds and preserve the integrity of your original documents. Compatible across nearly all Windows platforms, if you can print from a windows application you can use pdfMachine.

Get yours now!